IEEE Access
Multidisciplinary ⋮ Rapid Review ⋮ Open Access Journal

Received 19 September 2023, accepted 12 October 2023, date of publication 16 October 2023, date of current version 31 October 2023.

Digital Object Identifier 10.1109/ACCESS.2023.3325195

RESEARCH ARTICLE

Data-Driven Unified Scheme to Enhance the Stability of Solar Energy Integrated Power System in Real-Time

DIVYA RISHI SHRIVASTAVA[1], SHAHBAZ AHMED SIDDIQUI[2], KUSUM VERMA[3], (Senior Member, IEEE), SATYENDRA SINGH[4], MAJED A. ALOTAIBI[5], HASMAT MALIK[6,7], (Senior Member, IEEE), AND FAUSTO PEDRO GARCÍA MÁRQUEZ[8]

[1]Department of Electrical Engineering, Manipal University Jaipur, Jaipur 303007, India
[2]Department of Mechatronics Engineering, Manipal University Jaipur, Jaipur 303007, India
[3]Department of Electrical Engineering, Malaviya National Institute of Technology Jaipur, Jaipur 302017, India
[4]Faculty of Electrical Skills Education, Bhartiya Skill Development University, Jaipur 302037, India
[5]Department of Electrical Engineering, College of Engineering, King Saud University, Riyadh 11421, Saudi Arabia
[6]Department of Electrical Power Engineering, Faculty of Electrical Engineering, University Teknologi Malaysia (UTM), Johor Bahru 81310, Malaysia
[7]Department of Electrical Engineering, Graphic Era (Deemed to be University), Dehradun 248002, India
[8]Ingenium Research Group, Universidad Castilla-La Mancha, 13071 Ciudad Real, Spain

Corresponding authors: Hasmat Malik (hasmat.malik@gmail.com) and Majed A. Alotaibi (MajedAlotaibi@ksu.edu.sa)

This research was supported by the Researchers Supporting Project at King Saud University, Riyadh, Saudi Arabia, for funding this research work through the Project number RSP2023R278.

ABSTRACT Solar energy penetration in power grids helps to maintain power balance between generation and demand, thus enhances power grid performance. However, these integrations reduce grids' time margin to respond against sudden frequency changes and re-establishing generation-demand equivalency. Thereby, it poses challenges to the performance and stability of the power system. It therefore becomes increasingly important to comprehend the real-time system data, identify and initiate necessary remedies to sustain the healthy system's operation. This article presents a data-driven unified methodology for enhancing grid stability in solar energy-penetrated power network. The proposed method is a two-stage unified framework that incorporates Prompt Instability Evaluation (PIE) to evaluate impending system transient instability in first stage. In the second stage for a system unstable operation a Decision Assisted Adaptive Control (DAAC) is developed and implemented for corrective emergency control. A novel PIE is presented to perform a post-disturbance transient stability assessment using short-synchronized moving data. The PIE assesses the upcoming transient instability within the first few cycles following fault inception. Next, a novel DAAC is proposed to design an emergency remedial scheme for identifying location (where), magnitude, and type in real-time for unstable operations. The DAAC utilizes a novel Decision Rule Based Inference (DRBI) to evaluate suitable action sets that may be deployed by the DAAC to sustain system stability. The simulation results demonstrate the suitability of the proposed study on the system's performance in the absence/presence of solar energy with topological variations.

INDEX TERMS Decision assisted adaptive control, exponentially weighted moving average, solar energy, transient stability assessment.

I. INTRODUCTION

Globally, electricity demand is expanding at an unprecedented rate, and power networks have adapted by utilizing a mix of various energy sources to meet this growing demand. Renewable Energy Penetration (REP) to the existing power grids has achieved enormous attention of utility engineers, system operators and researchers in recent years. The REP at the key and critical locations enhances the performance of the power grid. Yet, integrating renewable sources to the system pose severe challenges to the real-time system monitoring, operation, and control of the systems. The capability

The associate editor coordinating the review of this manuscript and approving it for publication was Nagesh Prabhu.

to self-heal from emergencies, greater grid resiliency, and operating ease are critical characteristics for ensuring the reliability and continuity of electric power in REP integrated power systems [1]. This necessitates real-time network information, effective situational awareness, and an appropriate strategy for dealing with the emergent abnormal settings. Synchrophasor technology [2] transfers time-stamped synchronized wide-area network data. A suitable cluster of Phasor Measurement Units (PMU) is used in the technology to calculate the synchronized voltage and current phasor measurements.

The appropriate analysis and assessment of this synchronized data exhibits grid integrity and is becoming increasingly crucial for Renewable Energy Penetration (REP). REP not only diversifies the fuel utility but also contributes to the conservation of natural resources and improves energy security. Increased renewable penetration, on the other hand, pose challenges in grid operation due to a variation in system inertia. Any disturbance in the power network upsets the generation-demand equilibrium and, subsequently, changes the system frequency. The system inertia impacts the synchronous operation of the machines and assists the time-margin of power grids to respond to these arising imbalances [3]; however, integration of REP with no inertia such as solar energy with conventional grids decreases the system inertia. In the scenario of hybrid power generation, the synchronous generator's response to system disturbances in terms of rotor angles and speed deviations may degrade further. Under such circumstances, a large disturbance may drive the generator angles to advance more rapidly against the rest of the system. The fast advancement of the generator may lead its rotor to achieve an out-of-step state more rapidly. This state is generally described as transient instability. Therefore, post-disturbance power system Transient Stability Assessment (TSA), particularly incorporating solar energy integration, is critical for grid smooth operation.

In conventional power grids, machine-learning models in unison with wide area measurements are utilized to predict the generator's online dynamic behaviour [4]. The online dynamic analysis is more important for post-fault online system investigations and less feasible towards the real-time framework. Reference [5] proposes the Wide Area Transient Instability Severity Analyzer (WATISA) to early predict the severity imposed by an ensuing event. Although the assessment is timely, accurate, and model free, its suitability is limited to only conventional power systems. The transient potential and kinetic energy coupled with parametric space estimate the transient stability margins [6]. These estimates evaluate the region of attraction (ROA) encompassing the equilibrium solution set. The ROA is inversely proportional to system loading; therefore, it is not a suitable instability indicator. To approximate the transient stability boundary, literature also investigates critical clearing time (CCT) estimates, which signify the maximum allowable time to clear a fault. The mahalanobis-kernel regression [7] and generator-based threshold computation [8] are a few state-of-the-art methods to compute CCT for the generators. Cui et al. [9] present a combinational transfer learning strategy to improve TS prediction using convolutional neural networks.

A spatial distribution time adaptive methodology for predicting the transient stability status of the system is proposed in [10]. The time-adaptive framework is developed using several cycles of long-term memory classifiers, and a trust score is proposed for the reliability index. A time-delay neural network and bidirectional long short-term memory network-based data-driven TSA methodology is presented in [11]. Reference [12] proposes an active transfer learning-based approach that employs deep belief network maximum mean discrepancy. An improved deep belief network-based methodology incorporating structural characteristics of the network is proposed in [13]. To interpret the transient stability predictor outcomes, local linear interpreter model is also presented. A probabilistic transient stability assessment for wind energy integrated power grid is proposed in [14]. The scheme estimates the transient stability criterion using extreme learning machine and Gauss-Hermite integral based point estimation.

The early transient instability estimates, calculation of CCT/stability boundaries, and real-time stability assessments augment the situational awareness and determines the time instant to execute the emergency remedial strategy, if the system tends to approach unstable settings. In this regard, [15] presents an islanding and auto load shedding technique to stabilize the system and prevent blackout. Methodology utilizing voltage stability Index and load bus ranking [16] presents dynamic adaptive load shedding to ensure frequency resiliency in the power network. A unified approach to first assess the transient stability status and subsequently, implement preventive and emergency control strategy is proposed in [17]. The strategy utilizes synchronized voltage and angle measurements to predict the system instability and formulate the emergency actions: generator tripping and/or load shedding. The adaptive load shedding scheme based on voltage stability assessment [18], [19], combined frequency stability assessment and power flow tracing methodology [20] are utilized to enhance grid stability.

Unlike other power sources, solar energy integration has no effect on frequency-power equivalency but however reduces time margins and stability boundaries. Such power additions adversely impact grids' stability and therefore, the post-disturbance stability assessments are becoming more significant in these grids [20]. Adetokun et al. [21] explores P-V and Q-V based indices to improve voltage stability and enhance grid resiliency of large solar energy integrated power grid. The Quasi-Differential Search based SVC is investigated in [22] to improve transient instability. The approach enhances the oscillation damping, thereby decreasing the steady state settling time. However, it does not suggest the requisite strategy to augment the transient instability of

the system if post-disturbance, the network is tending to exceed the extreme settings. Wandhare et al. [23] showcases energy function assisted scheme to damp out low frequency power swings. The low frequency oscillations are system response to small or less severe disturbances. The power imbalance due to small disturbances are effectively damped out by power system stabilizers and other control schemes. These control schemes do not significantly damp out power swings arisen due to large or severe disturbance(s) and requires real-time remedial action schemes to preserve grid stability. To augment transit stability in renewable energy integrated power networks, fault current limiters are also utilized to supress the fault current and subsequently, improves of fault ride through capability [24]. Jawad et al. [25] proposes Battery Energy Storage System (BESS) assisted frequency stability enhancement of solar energy penetrated grid. Post-disturbance, BESS augments the power generation and provide a brief-support in maintaining system power balance. However, both the PV system and the BESS do not provide frequency support or system inertia, that otherwise further advances the already advanced generator from the rest of the network and eventually leads to out-of-step. Chandra et al. [26] recently presented synchronized measurements and a voltage stability index-assisted adaptive load shedding technique to maintain the steady-state frequency of a power network with solar park.

From the review of the literature, it can be concluded that the available methods and techniques for solar PV energy and conventional synchronous generator-based hybrid power generation either regain frequency stability through an emergency strategy or validate the integration of solar energy to the grid. To the author's best of knowledge, literature on improvement of power grid steadiness in terms of real-time TSA and, subsequently, deploying the emergency remedial strategy in real-time with solar energy penetration has not been reported. Thus, the investigation in this paper focuses on the effective monitoring, assessment and control of solar energy integrated power grid. First, Real-time prognosis of impending transient instability following the disturbance is investigated. Next, if necessary, the methodology ensures the transient stability of the PV integrated power system by framing and deploying corrective actions in real-time. The major contributions of this paper are summarized as:

1. First, Prompt Instability Evaluation (PIE) is developed to accomplish early transient stability assessment of the grid having high solar energy penetrations. The highlight of PIE is its ability to identify time-instant of the emergency strategy initiation (if required). The PIE utilize short moving window of real power generated (including power from solar PV) by the power sources as input.
2. Next, subsequent to the PIE assessments, a novel Decision Assisted Adaptive Control (DAAC) is triggered to assess the type, location (where), and magnitude of actions for unstable operating scenarios of grid. The proposed DAAC encompasses Decision Rule Based Inference (DRBI) to identify and initiate set-of-actions at a suitable location.
3. To maintain transient stability of solar integrated power system and prevent the major portion of the system from collapse, the proposed composite scheme is an essentially response-based framework. Moreover, all the actions are implemented in real-time using synchrophasor measurements. Therefore, the proposed scheme has a generalization capability which finds application to any system (with or without solar energy sources) in a wide range of operational scenarios.

The proposed composite methodology is evaluated using a modified New England 39 Bus test system that incorporates solar energy. Fig. 1 illustrates an overall summary of the unified framework. The remainder of the paper is organized as: Section II describes the Prompt Instability Evaluation of impending transient system instability in presence/absence of solar energy. Section III describes the Decision Assisted Adaptive Control (DACC) strategy to control system stability and enhance grid performance. The results and discussion on the test system with/without solar energy penetration are discussed in Section IV. The conclusions of the investigations are presented in Section V. Fig. 2 illustrates the section wise structure of the paper.

II. REAL-TIME POWER SYSTEM STABILITY ASSESSMENT

The post-disturbance power system severity can be assessed by timely monitoring any one or more of bus voltage, frequency, and angles. This section presents a novel real-time transient stability assessment (TSA) of power systems with/without solar energy penetration. First, the mathematical formulation of power system dynamics with/without solar energy is detailed. Subsequently, the proposed methodology of prompt instability evaluation for imminent transient instability is presented.

A. POWER SYSTEM DYNAMICS

The electric power delivered by synchronous machine is [19]:

$$Pe_j = Pm_j - \left(\frac{2H_jS_j}{f_n}\right)\frac{df_{Gj}}{dt} \tag{1}$$

where, f_n is nominal frequency, Pe_j (MW) is electric power generated, Pm_j (MW) is mechanical power, H_j (MW.s/MVA) is inertia constant, S_j (MVA) is machine rating, and f_{Gj} is frequency of j^{th} machine. During equilibrium condition, electrical power equals the mechanical power and Eq (1) is thus modified as:

$$\frac{df_{Gj}}{dt} = 0 \rightarrow Pe_j = Pm_j \tag{2}$$

In steady state condition, rate of change of frequency equals zero. If the equilibrium is disturbed during transient conditions, the rate of change in frequency can be either positive, indicating a decrease in electrical output, or negative, suggesting an increase in real power output and is given

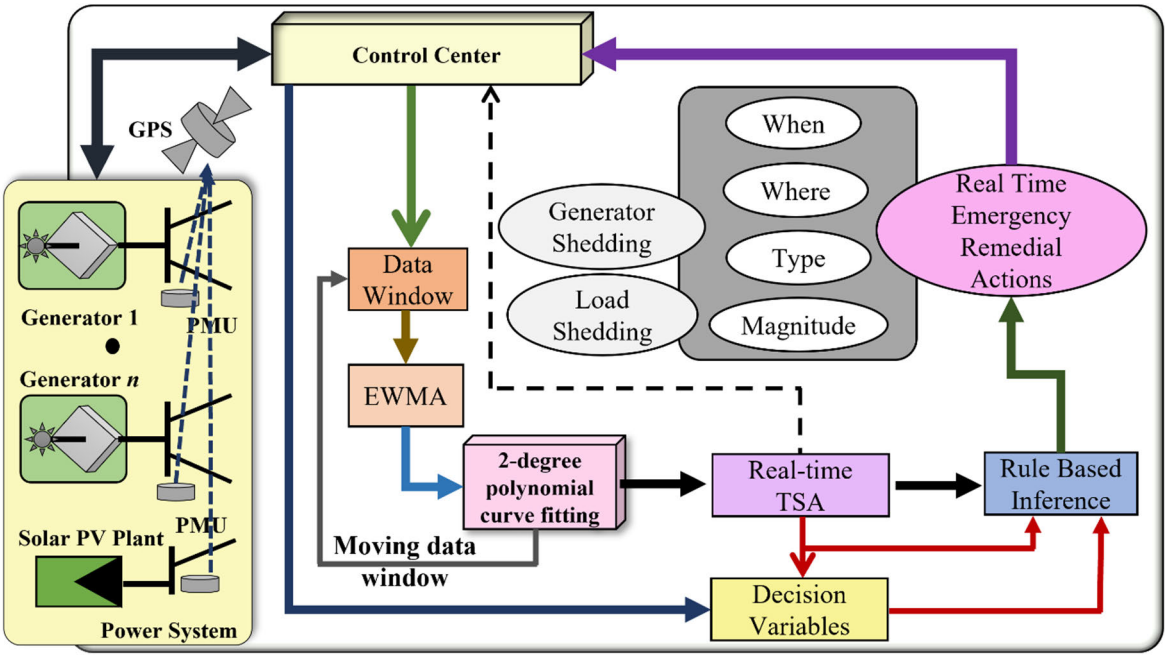

FIGURE 1. Overall summary of the proposed unified scheme.

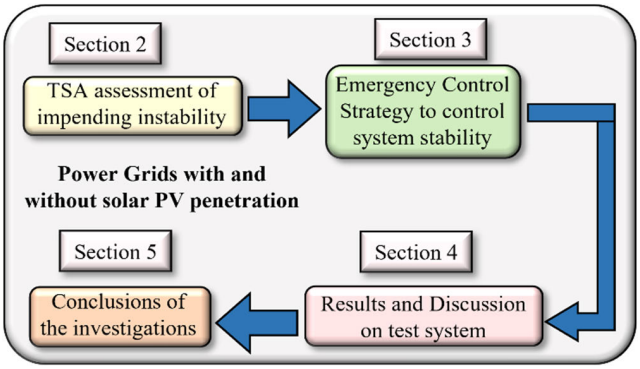

FIGURE 2. The section wise structure of the paper.

as:

$$\frac{df_{Gj}}{dt} > 0 \Rightarrow Pe_j \downarrow$$
$$\frac{df_{Gj}}{dt} < 0 \Rightarrow Pe_j \uparrow \quad (3)$$

The combined generated power (Pe) delivered by n machines is:

$$Pe = \sum_{j=1}^{n} Pe_j \quad (4)$$

The total system inertia based on the individual generator inertia constant and rated MVA power is calculated as:

$$H = \frac{\sum_{i=1}^{n} H_i S_i}{\sum_{i=1}^{n} S_i} \quad (5)$$

The PV system does not use a spinning mechanism to generate electricity. Thus, the solar farm's power does not have power-frequency equivalency. Furthermore, this integration adds no inertia to the system; rather, total inertia in the network reduces [3]. The decreased inertia lowers the critical clearing time for machines, causing them to get out of synchronism. Solar energy penetration can be incorporated into the grid either by replacing conventional synchronous machine plants or into the areas without conventional generators. In the first scenario, Eq. (6) with $n'=n$, can be used to determine the total power supplied. In contrast, in the second case, the total power is calculated using Eq. (6) with $n' = n\text{-}PV$, where PV is the number of solar plants in the grid. The power delivered by a power system with n' power generating sources is:

$$Pe = \sum_{j=1}^{n'} Pe_j + P_{PV} \quad (6)$$

where, P_{PV} is power generated by the solar parks. The overall system inertia is reduced with SE and a decreased SG-based generation mix, and is computed as:

$$H' = \frac{\sum_{i=1}^{n'} H_i S_i}{\sum_{i=1}^{n'} S_i + S_{PV}} \quad (7)$$

where, S_{PV} is solar plants MVA from and H' reduced inertia.

B. PROMPT INSTABILITY EVALUATION (PIE)

One of the consequences of the ensuing event in the network is an angular separation of rotor angles amongst the

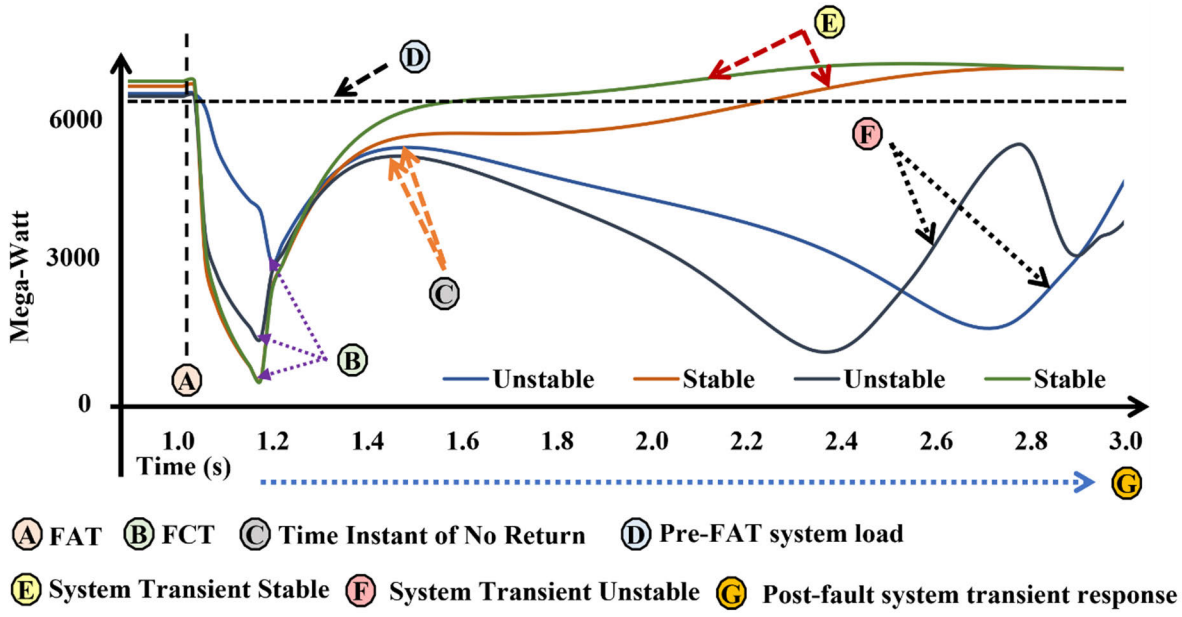

FIGURE 3. System power time series for transient stable and unstable operating scenario.

synchronous machines. In accordance with post-event system dynamics, an increase in power produced by an advanced generator tends to decrease the separation in rotor angles. At a specific time-instant, the increase in rotor angle of the accelerated generator decreases power supply, which may further lead the generator to fall out-of-step. The information of rotor angle separation in crucial for power system secure operation and is known as transient stability. Transient Stability is the rotor angle stability of the system to regain synchronism when subjected to large disturbance(s). Following the disturbance, prompt TSA assessment ensures sufficient time margin to formulate and deploy emergency control and augment grid sustainability. In this regard, timely, effective interpretation and valuation of short-synchronized data window is besought to estimate early TSA before the system actually exceeds the transient stability limits. Fig. 3 illustrates the variation of the total system active power for ensuing transient stable and unstable operating scenarios. This figure reflects that the variation in electric power is different for stable and unstable operating scenarios. Initially, the system is operating in equilibrium state such that rate of change of frequency is zero. At FAT, a severe fault (short circuit) occurs, resulting in disturbance of equilibrium and decreased generated power output from sources. Next, post-FCT, all the power sources tend to recover from the fault. Situations where the system power recovers and re-stablishes equipoise, results in transient stable system. Few scenarios where at certain instant of time, the total system power starts decreasing, the system will be moving to transiently unstable operations.

Thus, the total system power variations possess crucial information of transient stability of the system and therefore power variations can be utilized for identifying state of the system. Henceforth, continuous investigation of total generated power short-data window can be utilized to assess the estimations of awaiting instability. The short data window ensures fast response of system's instability status. However, long data window may provide more better estimation but have a large response time; such that, the system will already advance towards extreme settings leading to complete collapse. Thus, there is a trade-off between accuracy and response time, present short data length successfully appraises TSA in adequate response time for real-time applications. Fig. 4 displays the procedure utilizing a time series of generator rotor angle and total active power. The figure exhibit's fault initiation, clearance, three-cycle moving average of power data window, time-instant of no return T, early transient instability detection, time of detection (t_d), and available time margin to assess and deploy remedial measures. The mathematical formulation of the proposed PIE is detailed below. Let, Pe_{DW} be three-cycle window of generated power in the power system through Eq (6) as:

$$Pe_{DW} = [Pe(t_i)Pe(t_{i+1})Pe(t_{i+2})] \quad \forall t\varepsilon[FCT + 1cycle, t_d] \tag{8}$$

The moving data window of generated total power is employed to acclimatize the power system dynamics in real-time. Exponentially Weighted Moving Average (EWMA) is used for this purpose. EWMA [27], [28] is a statistical approach to remove noise (random fluctuations) and prioritizing recent measurements. Such that, recent measurements are weighted substantially higher than the preceding data to determine real-time system dynamics. For t^{th} time sample, the filtered data points can be calculated through Eq (9) and

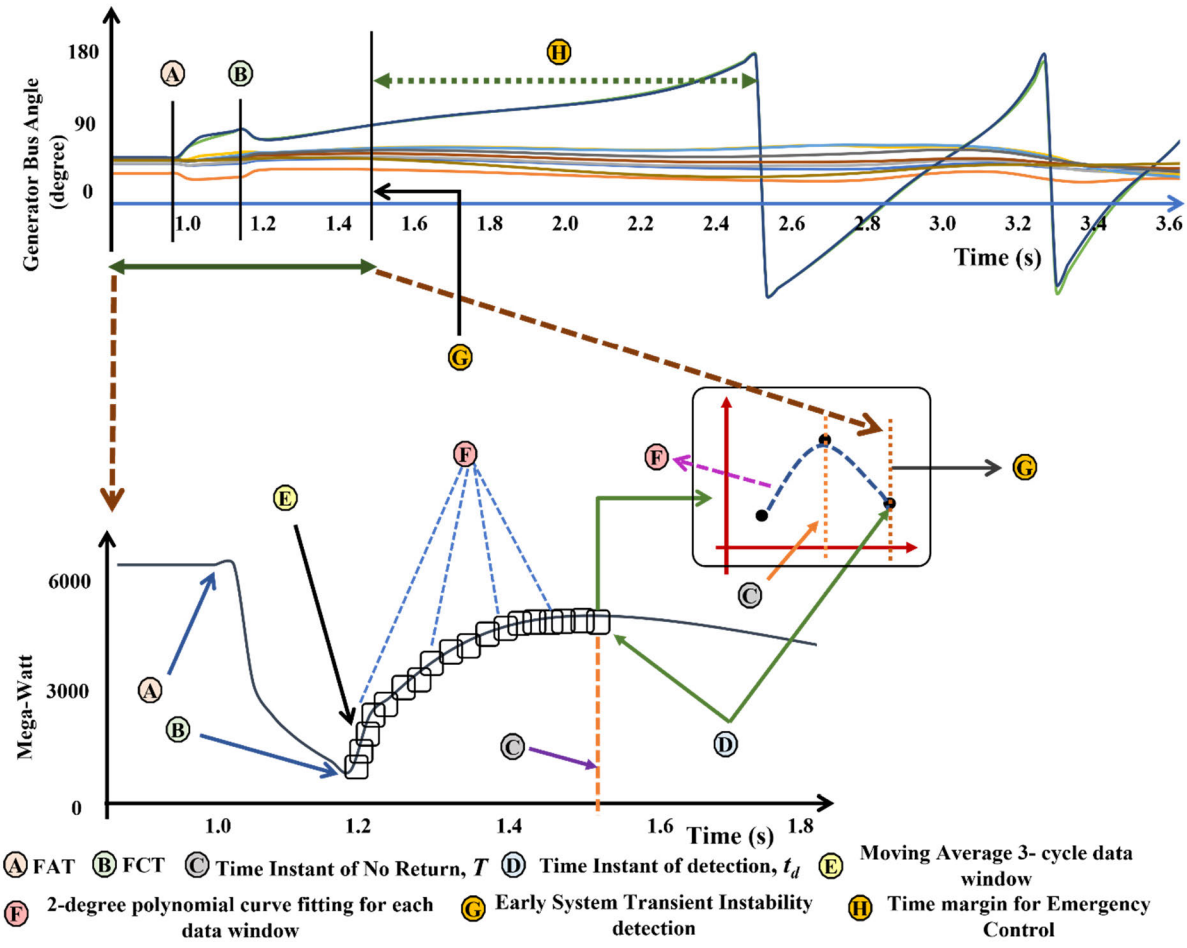

FIGURE 4. Proposed power system transient instability assessment.

weighing factor α is calculated through Eq (10) as:

$$Pe'[t] = \alpha Pe[t] + (1-\alpha)\, Pe'[t-1] \tag{9}$$

$$\alpha = \frac{2}{span+1} \tag{10}$$

In this work, span equals two data samples. The processed three cycle data available from Eq (9) is applied to 2-Degree polynomial fitting by minimizing the least squared error:

$$\min(E) = \min \sum_{m=1}^{3} |p(x_m) - Pe'_m|^2 \tag{11}$$

The Eq (12) is utilized to validate the maxima within 2-degree polynomial of the form:

$$p(x) = c_0 + c_1 x + c_2 x^2 \tag{12}$$

The maxima ensure the time of no return, that is, post-fault, the system does not tend towards recovery mode. Alternatively, within next few cycles, it will exceed transient unstable settings. Hence, at this step we are able to identify viz. (a) system is in-advance predicted to be transient stable or unstable, (2) time of initiation of emergency control actions, as shown in Fig. 5. The immediate detection of unstable operating state of the system ensures sufficient time margin to assess and deploy the wide area emergency remedial actions in real time.

III. REAL-TIME WIDE AREA EMERGENCY REMEDIAL STRATEGY

This section details the proposed real-time emergency action strategy appropriate for power systems with /without solar farm. The approach incorporates Decision Assisted Adaptive Control (DAAC) that leverages network real-time data to develop appropriate procedures. To sustain system stability, DAAC identifies action type (what), location (where), and magnitude based on a set of inference rules.

A. DECISION ASSISTED ADAPTIVE CONTROL (DAAC)

The real-time instability detection in the last section by PIE triggers the Decision Assisted Adaptive Control (DAAC). The DAAC computes the decision variables utilized by inference rules to identify the action type, location, and magnitude in the proposed strategy. These decision variables estimate the individual generator and system power imbalance and are based on real-time network information. As the DAAC

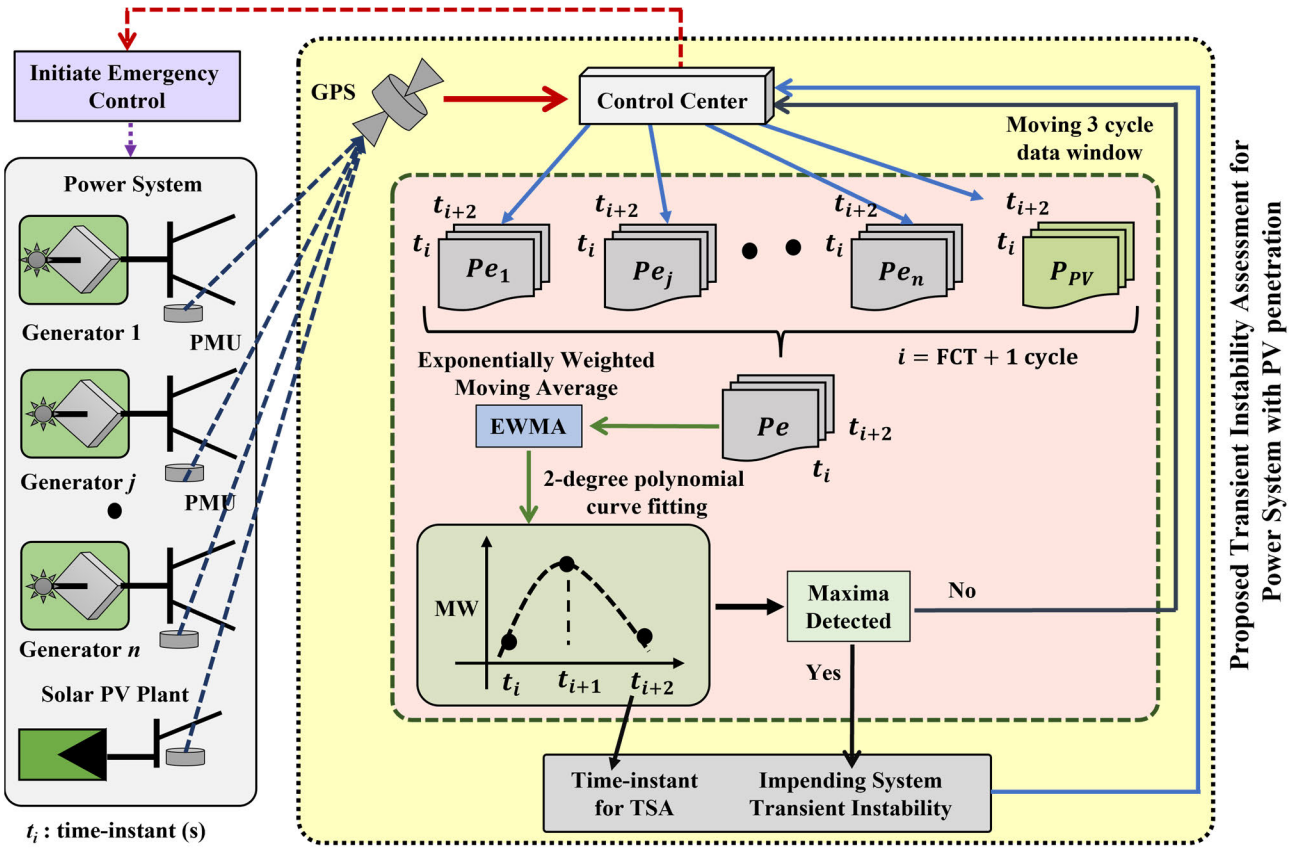

FIGURE 5. Overall summary of prompt instability evaluation.

is network data-driven, it is adaptive to system's topological and functional variations. Subsequent to PIE assessment, for j^{th} machine and at the time instant of PIE assessment, synchronized generator frequency along with MVA rating (S) and generator inertia (H), estimates the generator power imbalance dPg_j as:

$$dPg_j = \left(\frac{2H_jS_j}{f_n}\right)\frac{df_{Gj}}{dt} \forall j \varepsilon n \tag{13}$$

Summation of Eq (13) for all the n machines (n'in case of solar energy penetration) in power grid, estimates the total system power imbalance $delP$ as:

$$delP = \frac{2}{f_n}\sum_{j=1}^{n} H_jS_j\frac{df_{Gj}}{dt} \tag{14}$$

Although the generator frequency is qualitatively identical to the frequency of the node to which it is connected, the effect of interconnected nodes and local loads results in a small numerical difference. These trivial differences are utilized to estimate individual machine power imbalance. Thus, for j^{th} machine, estimated power imbalance due to frequency of the node connected to the machine is:

$$dPg_j^F = \left(\frac{2H_jS_j}{f_n}\right)\frac{df_{Gj}^F}{dt} \tag{15}$$

where, f_{Gj}^F is frequency of generator node and dPg_j^F is estimated power imbalance due to node frequency for j^{th} machine. The calculation of Eq (13) – (15) performed for single time instant, not only facilitates the fast identification of remedial solutions, but also decreases memory utilization for the power data processors located at centralized control centres. These power imbalances are taken as input to Decision Rule Based Inference (DRBI) to find the appropriate ''type, location and magnitude'' of the actions. The overall implementation of DAAC is summarized in Fig. 6.

B. DECISION RULE BASED INFERENCE

To endure system synchronism under abnormal scenarios a novel strategy Decision Rule Based Inference (DRBI) is proposed. *DRBI,* in its initial step, determines the type of action (What) to be employed. At time instant T, if any generator in the network is supplying excess power such that it is accelerating against the rest of the system, it is necessary to reject that generator from the system. The rejection of generation may cause other machines to share the power imbalance in proportion to their respective inertias. However, generator rejection has to be supplemented by load shedding, as it may still give rise to a power imbalance in the system. Therefore, relative load shedding is to be initiated to balance the generation-load imbalance. In contrast, load shedding is proposed if the load demand exceeds the power output from generators, affecting one of the machines to slow down in comparison to the rest of the system. The power imbalance

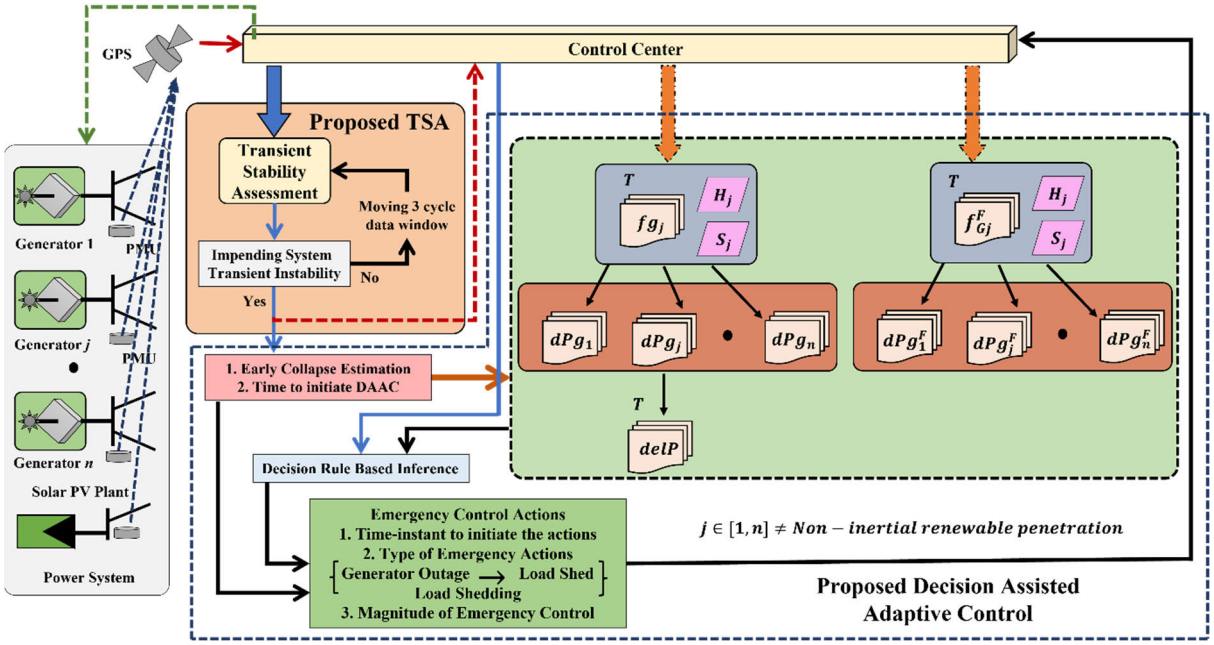

FIGURE 6. Proposed real-time emergency control strategy.

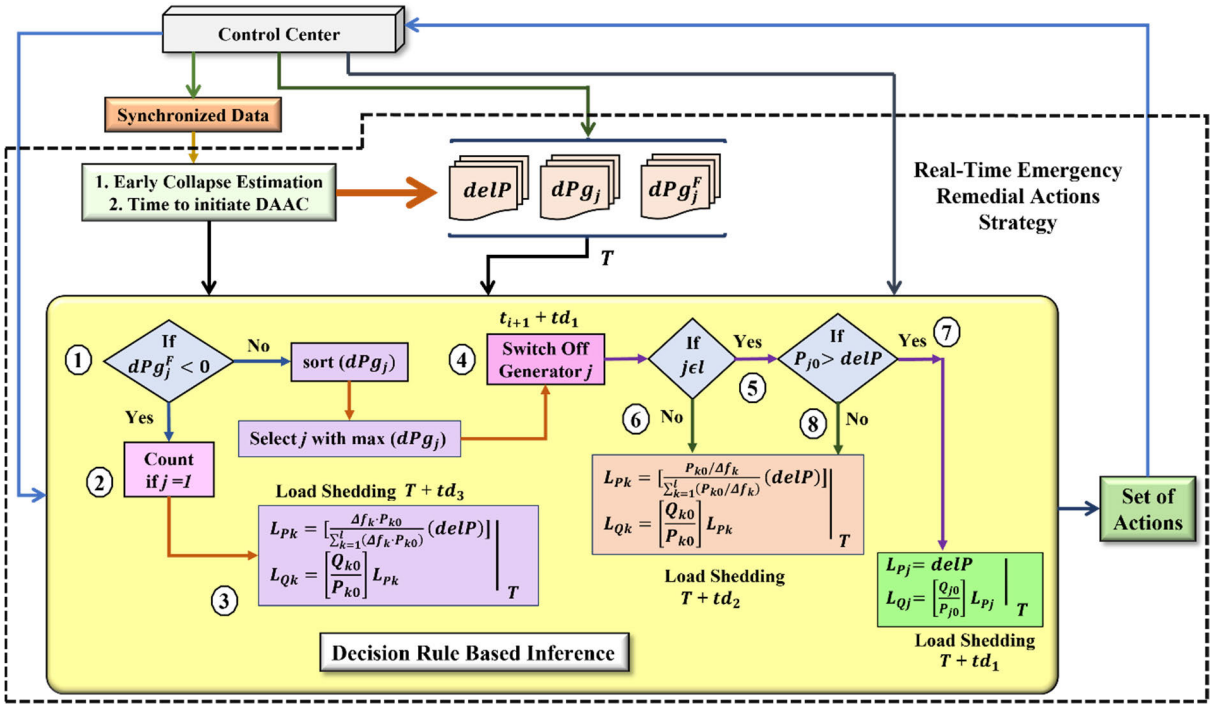

FIGURE 7. Proposed decision rule based inference (DRBI).

estimate computed through Eq (15) serves the decision variables for deciding the control action type: generator tripping and/or load shedding as:

$$dPg_{jT}^{F} \rightarrow \left\{ \begin{array}{l} < 0 \rightarrow \ LoadShedding \\ > 0 \rightarrow \ GeneratorRejection \end{array} \right\} \quad (16)$$

The negative estimates of dPg_{jT}^{F} for any generator infer the increased load demand. The set of actions corresponding to load curtailment is necessary to sustain stability. Alternately, positive estimates for all generators indicate excess power generation and it necessitates generation rejection followed by proportional load shedding. Fig. 7 highlights the suitable action type (What), location (Where), and magnitude (How) following the calculation of Eq (16). In the proposed DRBI, the set of actions as a stepwise approach are labelled as Action Set (AS) and are highlighted in Table 1. These Action Sets indicate the step-by-step approach to be adopted among each action type, the appropriate location and magnitude for

TABLE 1. Action set in proposed DRBI.

Action Type	Action type in Proposed DRBI	Stepwise approach (Action Set)
Generator Rejection	Generator Tripping	$AS^{(1)} \rightarrow AS^{(4)} \rightarrow AS^{(5)} \rightarrow AS^{(7)}$
	followed by Load curtailment	$AS^{(1)} \rightarrow AS^{(4)} \rightarrow AS^{(5)} \rightarrow AS^{(8)}$
	[$AS^{(1)} \rightarrow AS^{(4)}$]	$AS^{(1)} \rightarrow AS^{(4)} \rightarrow AS^{(6)}$
Load Shedding	Load Shedding [$AS^{(1)} \rightarrow AS^{(2)}$]	$AS^{(1)} \rightarrow AS^{(2)} \rightarrow AS^{(3)}$

$AS^{(1)}$: Identification of action type; $AS^{(2)}$: Decision of load shedding; $AS^{(3)}$: Calculation of magnitude for load shedding; $AS^{(4)}$: Detection of location for generator rejection; $AS^{(5)}$: Post generator rejection, detection of location of load shedding ; $AS^{(6)}$: Calculation of magnitude for load shedding ; $AS^{(7)}$: calculation of magnitude for load shedding; $AS^{(8)}$: Post generator rejection, calculation of magnitude for load shedding.

necessary remedial measures. Each of these action set is detailed in the following sub-sections.

1) GENERATOR TRIPPING: ACTION TYPE $AS^{(1)} \rightarrow AS^{(4)}$

a: LOCATION IDENTIFICATION

As the generator rejection decision is indicated, the location of the generator to be tripped is assessed. Since generation rejection is the consequence of increased generation in the system, the generator with excessive power generation among n machines is the candidate generator to be tripped. Apparently, the machine with the maximum imbalance contributes most to surplus generation. Its rejection will suitably ease the imbalance in the system. Thus, at time instant T, Eq (17) is sorted in descending order to identify the individual generator maximum power imbalance. The candidate generator with maximum imbalance (say j^{th} generator) is to be rejected. The process of identifying the candidate generator to be tripped, is represented as,

$$sort(dPg_j|_T) \Rightarrow max\left[\left(\frac{2H_jS_j}{f_n}\right)\frac{df_{Gj}}{dt}|_T\right] \forall j \varepsilon n \qquad (17)$$

b: MAGNITUDE AND LOCATION OF LOAD CURTAILMENT

The surplus power generation prior to generator rejection indicates a low power demand at load sites at time-instant of instability detection. Following the generator rejection, curtailment of large load buses may manifest an increased power demand from the system. Thus, it is imperative to identify the buses with light loads and curtail the adequate magnitude in real-time. Considering this fact, a new Load Sharing Index (*LSI*) has been developed in this work to identify the percentage share of total system load being shared by individual load bus. It basically calculates the share of individual load based on frequency deviation against nominal frequency at T. The deviation is then normalized by the cumulative deviation for all the load sites to obtain the percentage share. After tripping the identified generator, for the system with l loads, *LSI* for k^{th} load is calculated as,

$$LSI_k = \frac{f_k|_T - f_n}{\sum_{k=1}^{l}(f_k|_T - f_n)} \text{x} 100 \; \forall \; k \; \varepsilon l \qquad (18)$$

where, $f_k|_T$ is k^{th} load bus frequency at time T and f_n is nominal frequency. Following the generator trip, the numerical valuations from *LSI* are then utilized to estimate the location of load sites for load curtailment.

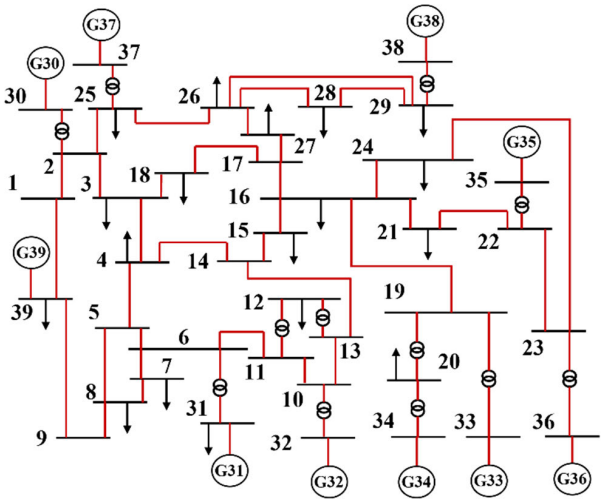

FIGURE 8. IEEE 39 bus test system.

TABLE 2. Detailed data generation.

Event Category	Stable Cases	Unstable Cases	Total Cases
N-2 contingency leading to bus isolation	78	50	128
Short circuit cleared with line outage	29	4	33
Cascaded faults	25	8	33
Total Cases	132	62	194

N: Number of lines.

c: ACTION SET AS $^{(1)} \rightarrow AS^{(4)} \rightarrow AS^{(5)} \rightarrow AS^{(7)}$

The *LSI* for all the loads is sorted to identify the least load sharing node.

If the load bus is same as that of the tripped generator and that the load pre-disturbance magnitude exceeds estimated imbalance *delP* at T time-instant, the equivalent magnitude L_{Pj} from this candidate load bus is curtailed. The electrical loads are in general characterized into two components: real and reactive. It is impractical to consider only real component for load shedding. Therefore, it is essential to shed the adequate quadrature component of the load. The reactive component L_{Qj} to be shed is calculated in proportion to the ratio of pre-disturbance reactive and real power component and L_{Pj}. Overall, the set-of-actions for this strategy is labelled as $\mathbf{AS^{(1)} \rightarrow AS^{(4)} \rightarrow AS^{(5)} \rightarrow AS^{(7)}}$. Thus, the necessary magnitude of candidate load to be shed is calculated as,

$$\left.\begin{matrix} L_{Pj} \\ L_{Qj} \end{matrix}\right\} \Rightarrow \left.\begin{matrix} |delP|_T \\ \left[Q_{j0}/P_{j0}\right] L_{Pj} \end{matrix}\right\} \forall \; j \; \varepsilon \; l \qquad (19)$$

where, for j^{th} location, L_{Pj} is active power and L_{Qj} is reactive power of the candidate load to be shed, P_{j0} is pre-disturbance active power, Q_{j0} is pre-disturbance reactive power for j^{th} load.

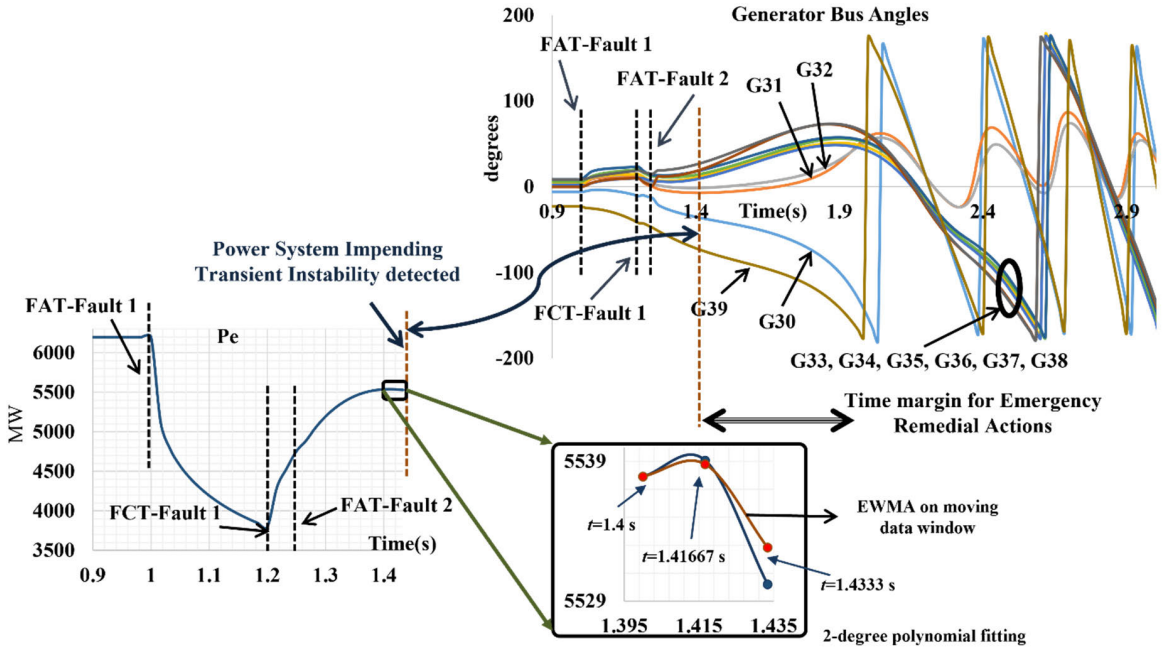

FIGURE 9. Proposed TSA for illustrative example I.

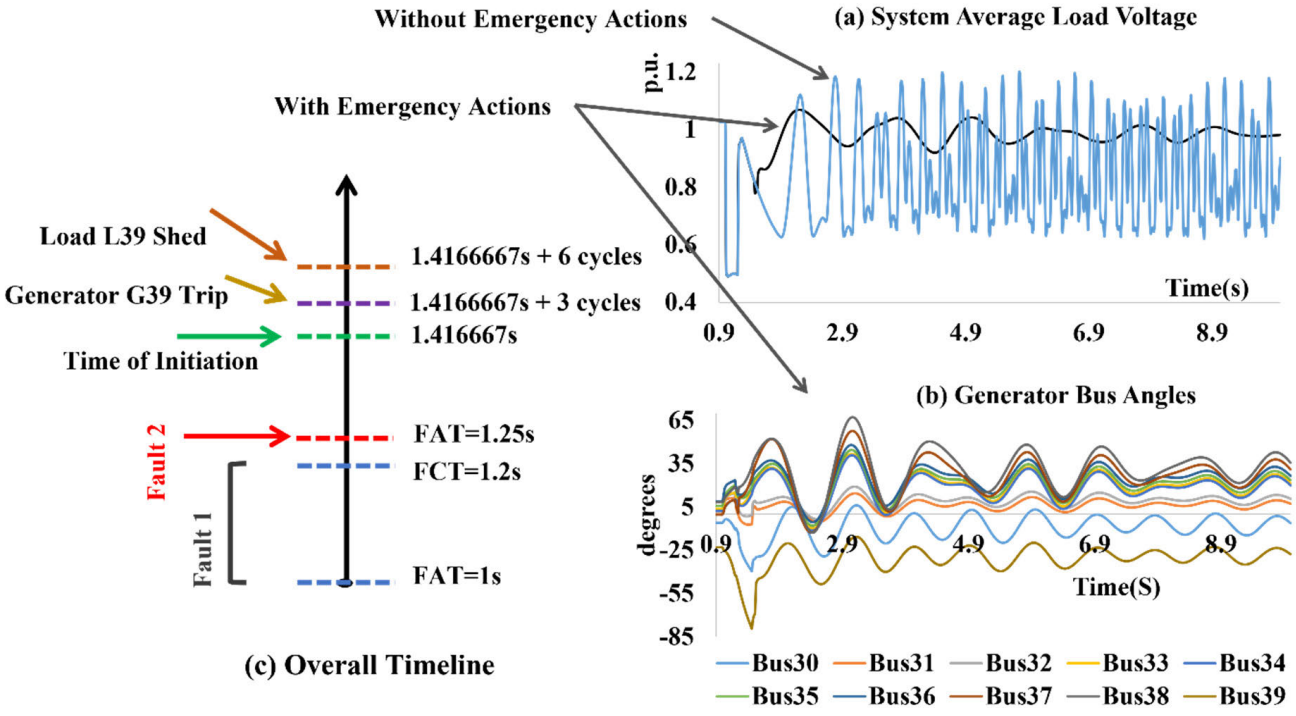

FIGURE 10. Outcome of three cycle delayed emergency remedial strategy for illustrative example I.

d: ACTION SET AS(1)→ AS(4) → AS(5) → AS(8) AND ACTION SET AS(1) → AS(4) → AS(6)

Alternatively, if the identified *LSI* calculation suggest the load bus that is not the same as of tripped generator ($j \notin l$) or, if the pre-disturbance magnitude load at j^{th} location is less than that of the estimated power imbalance ($P_{j0} < delP$); each load in the network is considered as a candidate load for load shedding. The magnitude L_{Pk} of the load to be curtailed is decided based on frequency deviation of the candidate load bus at T time-instant, pre-disturbance load amount, and power imbalance. The load with smaller frequency deviation from nominal frequency and a less pre-disturbance loading shares the major component of load shedding. Similarly, the reactive component L_{Qk} to be shed is calculated in proportion to ratio of pre-disturbance reactive and real power component, and L_{Pk}. Overall, the set-of-actions for the

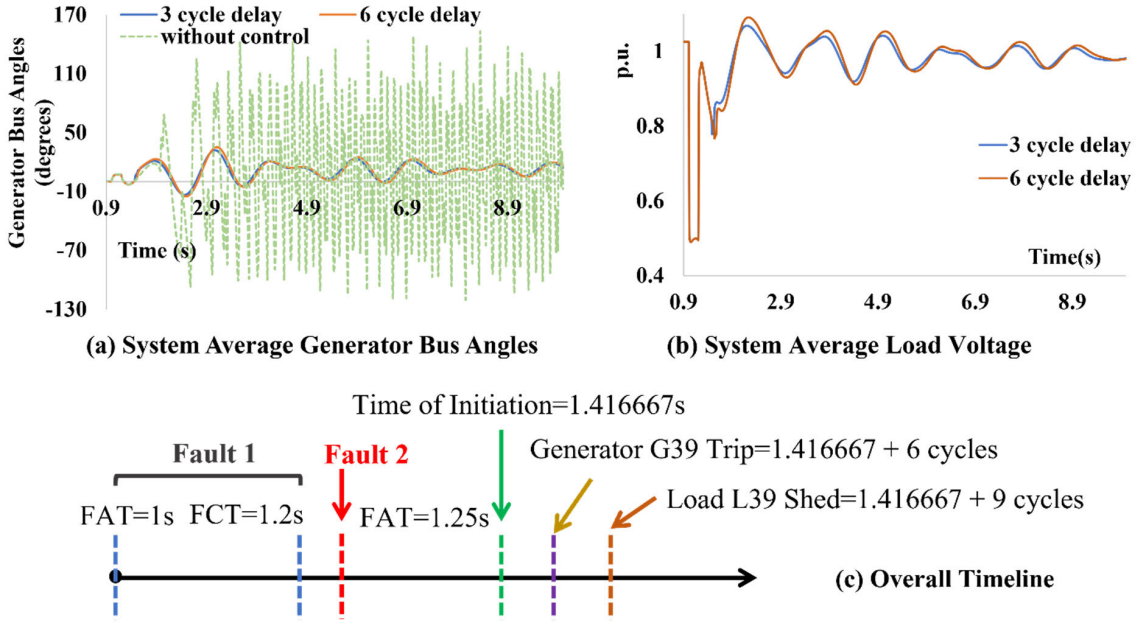

FIGURE 11. Impact of additional three cycle delayed Emergency Remedial Strategy for illustrative example I.

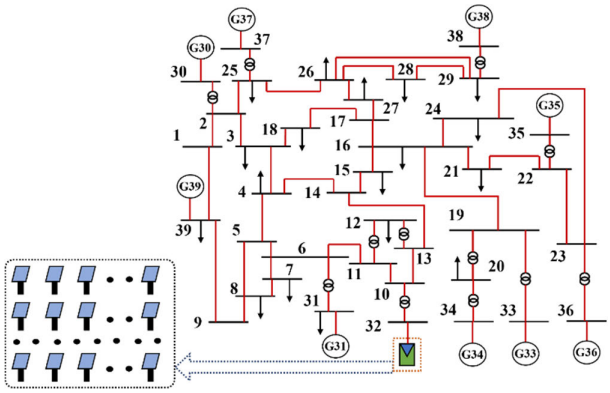

FIGURE 12. Modified new england 39 bus system with conventional generator replaced by solar farm at Bus 32.

situation ($j \notin l$) is labelled as $\mathbf{AS^{(1)}} \rightarrow \mathbf{AS^{(4)}} \rightarrow \mathbf{AS^{(6)}}$, while the action strategy for the situation ($P_{j0} < delP$) is labelled as $\mathbf{AS^{(1)}} \rightarrow \mathbf{AS^{(4)}} \rightarrow \mathbf{AS^{(5)}} \rightarrow \mathbf{AS^{(8)}}$. In both instances, the magnitude of load to be shed from all the load in the system is calculated as,

$$\left.\begin{matrix} L_{Pk} \\ L_{Qk} \end{matrix}\right\} \Rightarrow \left.\begin{bmatrix} \left(\left(\frac{P_{k0}}{\Delta f_k}\right) delP\right) / \sum_{k=1}^{n} \left(\frac{P_{k0}}{\Delta f_k}\right) \\ \left[\frac{Q_{k0}}{P_{k0}}\right] L_{Pk} \end{bmatrix}\right|_T \forall k \varepsilon l \quad (20)$$

where, for k^{th} load, L_{Pk} is active power and L_{Qk} is reactive power to be curtailed, P_{k0} and Q_{k0} is pre-disturbance active and reactive power, and Δf_k is the frequency deviation against nominal frequency.

2) LOAD SHEDDING: ACTION TYPE $AS^{(1)} \rightarrow AS^{(2)}$

a: ACTION SET $AS^{(1)} \rightarrow AS^{(2)} \rightarrow AS^{(3)}$

At the instant of instability detection, the negative power imbalance depicted by Eq (16) showcases the excess power demand. This additional power demand is numerically equivalent to the estimated power imbalance. Under this scenario, one or more generators may slow down. In the operational scenario of a single generator being slow down, all loads in the network are labelled as candidate loads. In proposed *DRBI*, these adopted set-of-actions are labelled as $\mathbf{AS^{(1)}} \rightarrow \mathbf{AS^{(2)}} \rightarrow \mathbf{AS^{(3)}}$. To distribute the imbalance among the loads, frequency change methodology [19] is utilized to calculate the magnitude of load shedding and is calculated by:

$$\left.\begin{matrix} L_{Pk} \\ L_{Qk} \end{matrix}\right\} \Rightarrow \left.\begin{bmatrix} (P_{k0} \cdot \Delta f_k \cdot delP) / \sum_{k=1}^{n} P_{k0} \cdot \Delta f_k \\ \left[\frac{Q_{k0}}{P_{k0}}\right] L_{Pk} \end{bmatrix}\right|_T \forall\, k\ \varepsilon\ l \quad (21)$$

where, at k^{th} location, Δf_k is the frequency deviation against nominal frequency, L_{Pk} is active power, L_{Qk} is reactive power to be shed. The frequency dependent strategy for load shedding distribution among the candidate loads, depends on individual load pre-disturbance numeric value and load bus frequency. Such that, a load with greater frequency deviation from nominal frequency and more pre-disturbance loading, shares the larger component of load shedding.

C. ACTUAL TIME OF ACTION DEPLOYMENT

Although the instigation of emergency actions is signaled at the time of instability detection, the actual initiation of actions is delayed. The delay in deployment is due to various associated delays for executing corrective actions [29] including latency in communication to central logic, substations, power plants, delays due to circuit breaker operating time, and computer processing time. Thus, post T time instant,

TABLE 3. Comparative evaluation of the proposed PIE with state -of-art learning techniques.

S.no.	Technique	Number of Test Cases	Overall Accuracy Actual/ Estimated	False Alarm Actual/ Estimated	Missed Alarm Actual/ Estimated	Impending Instability (Y/N)	When to Initiate ECA (Y/N)	Time-instant of Action Quantity Calculation (Y/N)
1	Random Forest	39	39/38	24/24	15/14	Y	N	N
2	Multilayer Perceptron	39	39/37	31/30	8/7	Y	N	N
3	k-NN	39	39/38	28/27	11/11	Y	N	N
4	DT	39	39/38	28/28	11/10	Y	N	N
5	AdaBoost	39	39/38	25/24	14/14	Y	N	N
6	Proposed PIE	194	194/189	132/127	62/62	Y	Y	Y

TABLE 4. Emergency remedial scheme for illustrative example I.

Action Type and Location	Time (s)	Action Magnitude
TSA detection	1.417	*delP*=627.808 MW
Trip G 39	1.417 + td_1	Shed 1000 MW Power Generation
Load Shed L39	1.417 + td_3	Shed 36.76% Load of 1707.925 MW and 383.5 MVAr

TABLE 5. Emergency remedial scheme for illustrative example II.

Action Type and Location	Time (s)	Action Magnitude
TSA detection	1.4167	*delP*=600.334 MW
Shed All Loads	1.4167+td_2 (0.05 s)	Shed proportionate % load illustrated in Figure 17(a) with total load shed equal to *delP*

td_1, td_2, and td_3 are time delays in the actual initiation of control actions such that this delay corresponds to a specific Action Set.

IV. RESULTS AND DISCUSSION

This section validates the implementation of the proposed unified scheme on the IEEE 39 Bus test system with and without solar energy integration. The DIgSILENT Power Factory is utilized to perform the simulation of the test system. The test system conventionally has 39 nodes, 34 lines, 12 transformers, 19 loads, and 10 synchronous generator-based power sources with a base 6266.82 MVA generation and load of 6257.77 MVA and, as shown in Fig. 8 [5]. In this paper, real-time data is available with 1 sample/cycle (60 Hz sampling frequency). The performance of the proposed composite scheme is tested on generated database consisting of different faults with different system loading. The disturbances simulated are considered individually and in cascaded scenario and are categorized in stable /unstable scenarios. Table 2 illustrates the generated dataset comprising event category, unstable/stable cases and total cases. In the subsequent sections, first the performance scores of the proposed PIE and DAAC implementation are discussed. Next, execution of proposed strategy on test system in absence of solar farm is showcased through illustrative example I. Subsequently, to test suitability of the proposed scheme to enhance stability and avoid grid collapse on SE penetrated power system, one representative example with single SE penetration (illustrative example II) and illustrative example III with multiple bus SE penetration are employed. Finally, a comparative assessment of the presented work against available state-of-art is showcased. The proposed strategy is realized on a PC with Intel i5 CPU 2.4 GHz processor and 16 GB RAM.

A. PERFORMANCE EVALUATION OF PROPOSED PIE AND DAAC

A comparative evaluation of the proposed PIE scheme with the data-mining techniques available in literature is accomplished and is detailed in Table 3. The Table presents statistics regarding the count of cases that were incorrectly classified as stable (referred to as ''Missed Alarm'') and the count of cases that were incorrectly classified as unstable (referred to as ''False Alarm'') for each type of event. As is apparent, the proposed PIE for TSA provides multiple objectives, including predicting future instability, reducing the occurrence of false and missing alarms, and evaluating the time required to execute emergency actions. A comparative analysis has been performed to assess the effectiveness of machine learning approaches available in literature and the proposed PIE methodology for different cases.

The data mining techniques, in comparison to the proposed PIE, require training using 80% of the available data, while the remaining 20% is utilized for testing the models. However contrary to these techniques, the PIE approach does not employ learning models; instead, all the generated data is subjected to testing. The results indicate that the performance of the suggested PIE method in assessing the likelihood of impending system transient instability is superior. Upon identification of impending instability for the unstable cases in Table 3, DAAC is deployed to sustain system stability and augment power grid operation. The proposed control action strategy successfully augments grid performance and stability.

In the subsequent sub-sections, the performance of DAAC is displayed by two illustrative examples in the absence/presence of solar plant. Moreover, the performance of the composite scheme is also showcased on solar plant integration at multiple locations with an illustrative example.

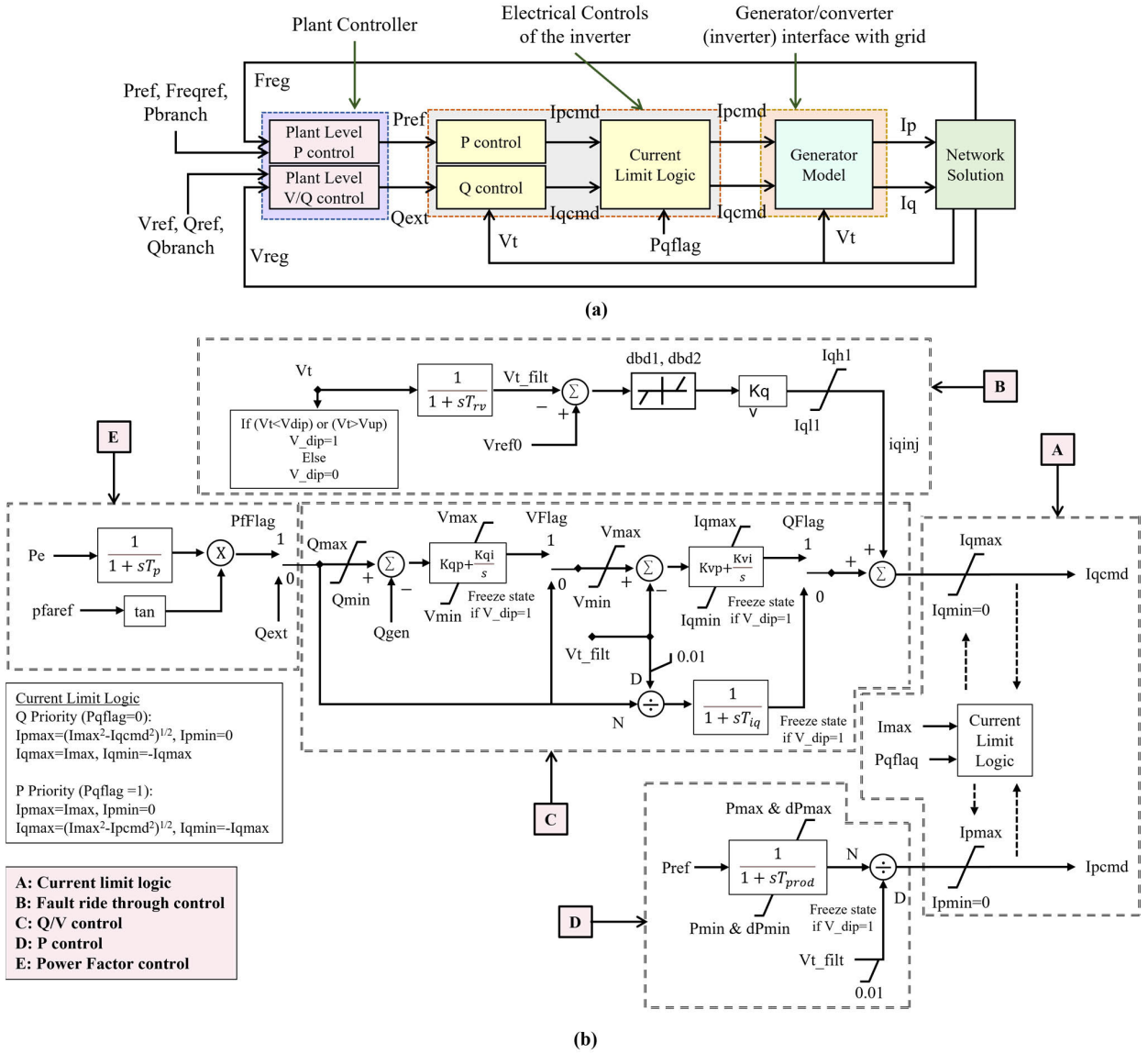

FIGURE 13. (a) The dynamic model of PV plant; (b) Electrical control model block diagram.

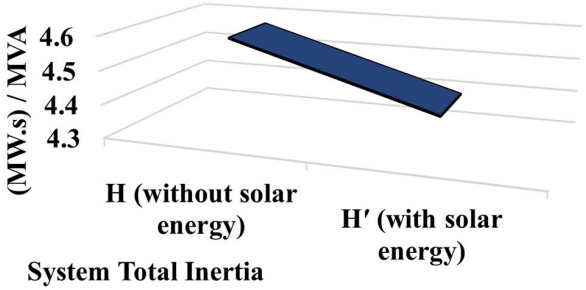

FIGURE 14. System inertia in presence and absence of solar energy penetration.

B. TEST RESULTS OF THE PROPOSED FRAMEWORK ON TEST POWER SYSTEM IN ABSENCE OF SE PENETRATION

In this section, the proposed scheme is employed on test system in absence of solar energy integrations. For this purpose, stepwise assessment on illustrative example I is showcased.

1) ILLUSTRATIVE EXAMPLE I: CASCADING EVENT SCENARIO

System loading: 101% of base case
Fault 1: Short Circuit near Bus 03
Fault 1 FAT=1s
Fault1 Cleared: FCT=1.2s by opening Line 03-18, and subsequently,
Fault 2: Line 02-25 Outage
Fault 2 FAT=1.25s

Example I is an illustration of cascaded events intended to comprehend the system response with and without the suggested unified methodology. Fig. 9 represents the generator(s) bus angles response to the consecutive faults. At 2 seconds, Generators G30 and G39 are clearly out-of-phase with the event 1 post-fault clearance and the simultaneous onset of event 2. This transient instability spreads to the remaining generators, and G33-G38 are out of synchronization during the following few cycles (about 2.6 seconds), the system

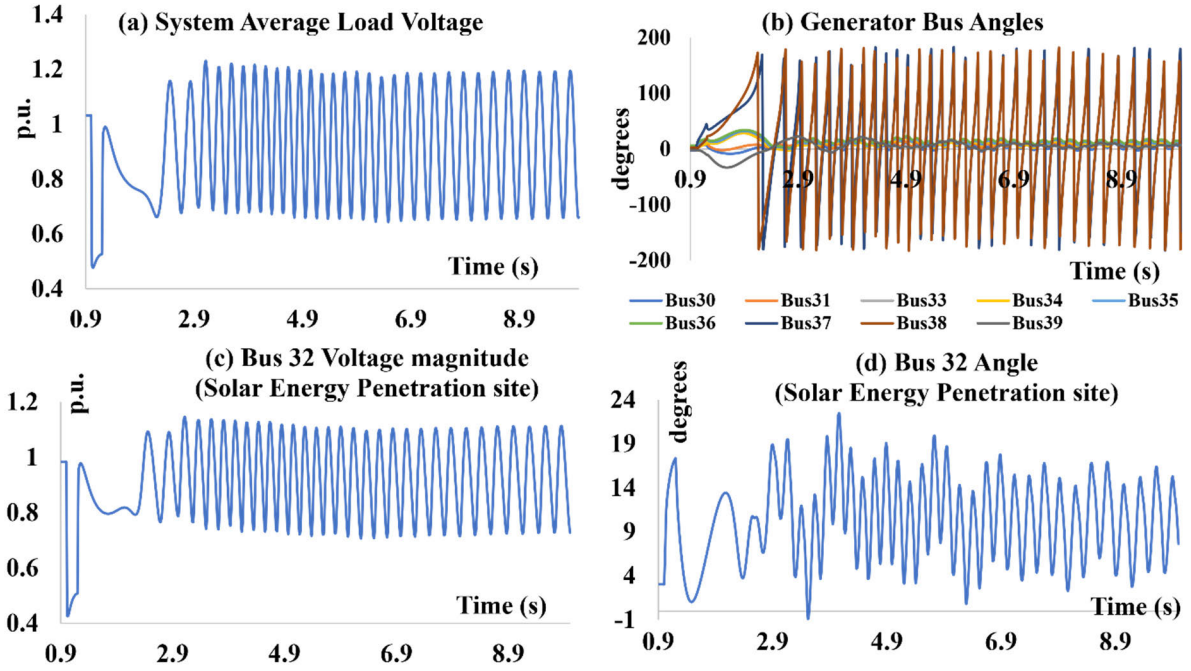

FIGURE 15. Illustrative Example II: without emergency remedial strategy.

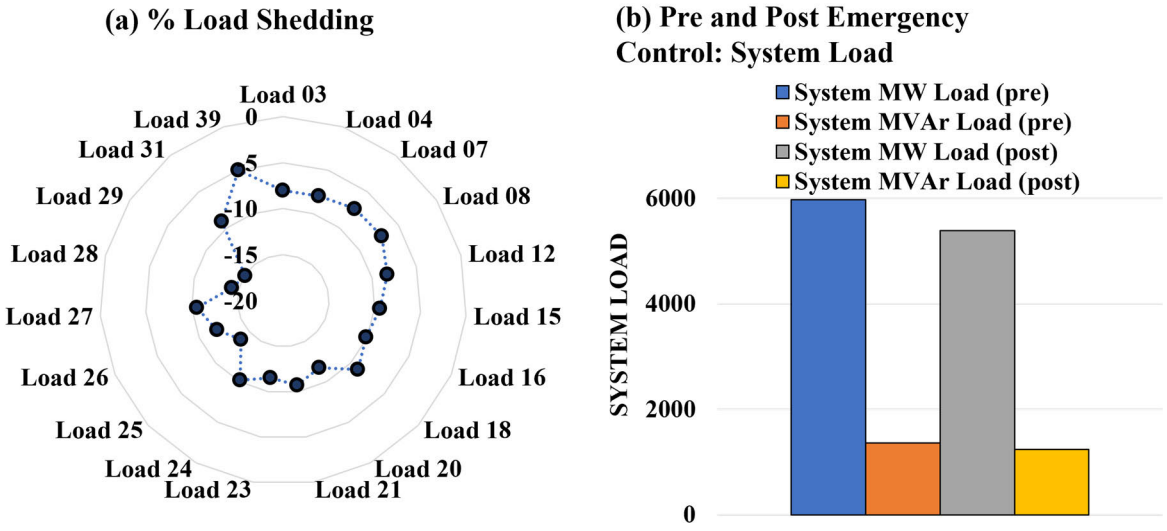

FIGURE 16. Illustrative Example II: load shedding.

collapses. To avert a blackout, it is critical to detect the instability early, formulate, and execute emergency steps. The PIE module is initiated to estimate the forthcoming instability scenario. The PIE module identifies the impending transient instability settings at 1.417 seconds, allowing approximately 0.6 seconds to schedule and deploy an emergency control strategy. The proposed TSA indicate that (1) the system is transiently unstable; (2) the time of control initiation; and (3) DAAC implementation is flagged. The proposed Emergency control strategy computes the action type, location, and magnitude tabulated in Table 4. The action type $AS^{(1)} \rightarrow AS^{(4)}$ that is generator rejection followed by load shedding is suggested with an appropriate magnitude of respective action. Due to different delays associated with deploying the remedial control strategy, the actual time of initiating emergency control is delayed.

The emergency control strategy effectively avoids grid collapse even with a 3-cycle (0.05 s) time delay, as evident from Fig. 10. The figure showcases the system average load voltage profile, generator bus angles, and overall timeline of the complete procedure. At times, due to network congestion, the delay in deployment may be more. In this regard, the remedial solution is deployed with an additional delay of 3 cycles (a total of 6 cycle delay) as shown in Fig. 11. The figure elaborates: effect of delays in deployment for system average load voltage, generator bus angle against no control

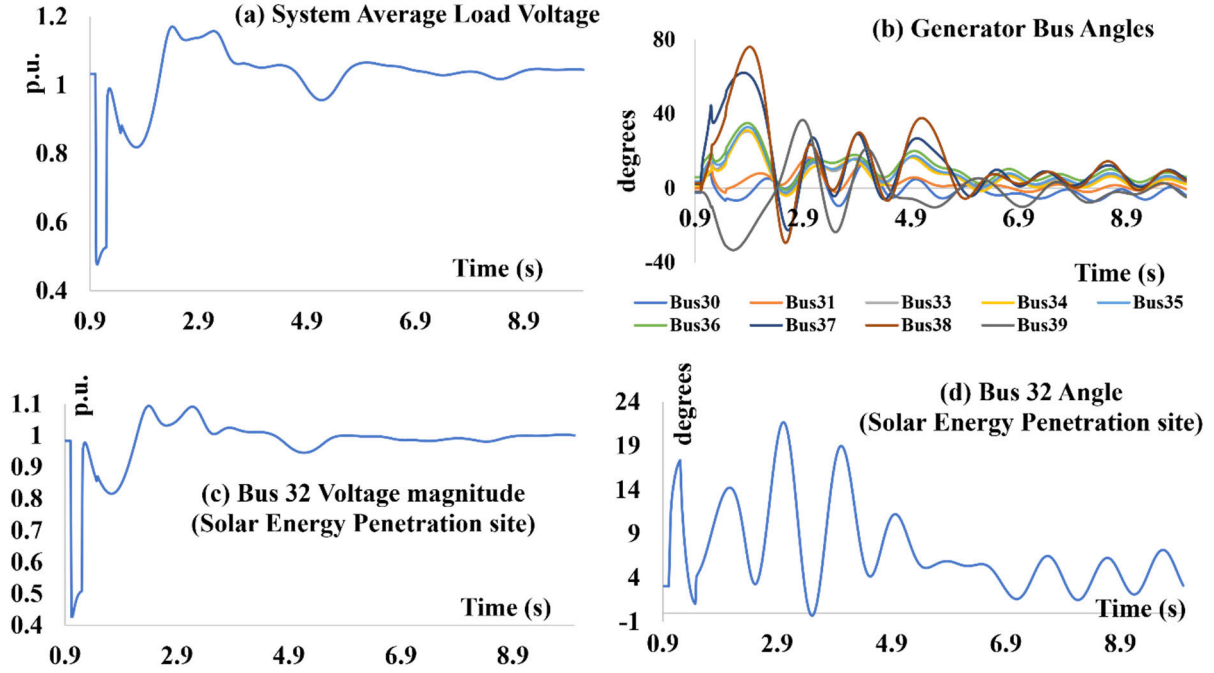

FIGURE 17. Illustrative Example II: with emergency remedial strategy.

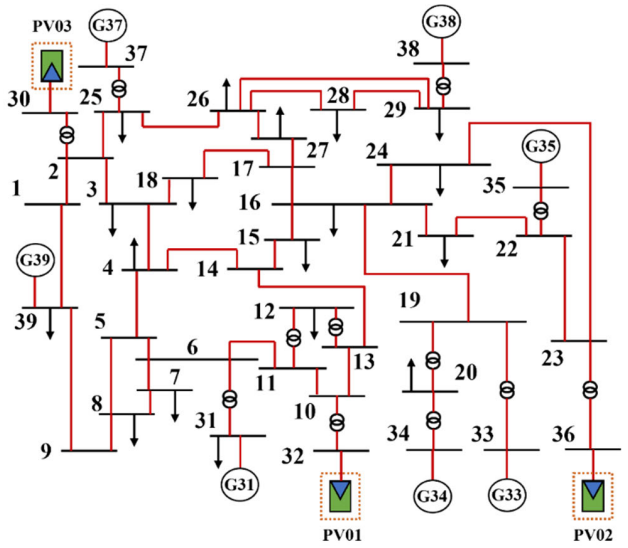

FIGURE 18. Modified new england 39 bus system with conventional generator replaced by solar farm at bus 30, bus 32, and bus 36.

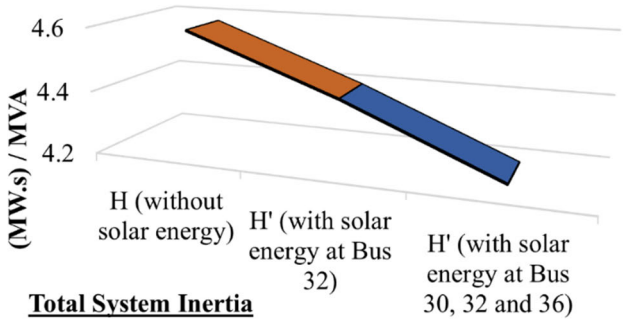

FIGURE 19. System inertia in absence and presence of solar energy penetration at single and multiple locations.

application, and overall timeline for the proposed composite scheme for 6-cycle delayed deployment. The results highlight that there is no significant variation in system voltage profile and generator angle for an additional time delay. Evidently, the results validate the applicability of the proposed unified strategy to mitigate transient instability and avoid grid collapse even under a series of faults.

C. TEST RESULTS FOR SOLAR ENERGY INTEGRATED POWER SYSTEM (SINGLE LOCATION)

This section examines the applicability of the proposed method on the test system that has been modified by solar energy integration. Fig. 12 demonstrates the modified test system with a solar PV farm replacing a conventional generator at Bus 32. The 650 MW solar PV farm with 50 columns and 20 rows, adding 1000 PV units; each unit has a 720 kVA 0.9 pf inverter that generates 650 kW of electricity. The dynamic model of a solar PV plant utilized in the study consists of (a) a plant controller, (b) electrical controls, and (c) a grid interface module [30]. The Plant Controller utilizes voltage and reactive power output to imitate var/volt control and frequency and active power output to follow active power control at the plant level. The power output acts as a reference to the electric control model to give real and reactive current as output and terminal voltage and generated power as feedback. The real/reactive currents are utilized by the grid interface module to process and inject real/reactive current into the grid. The overall layout of the dynamic model is outlined in Fig. 13 (a). The faster active power recovery (fault ride through capability) of PV inverters indicates the response of PV inverter against voltage sags due to grid disturbances.

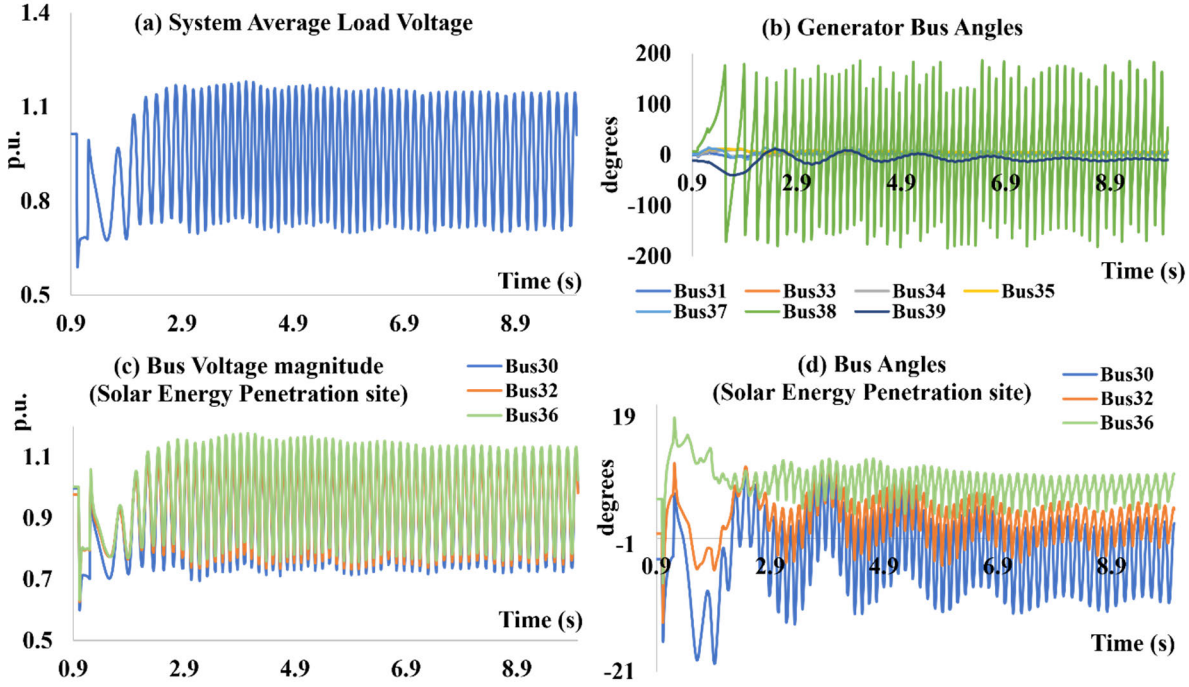

FIGURE 20. Illustrative Example III: without emergency remedial strategy.

TABLE 6. Emergency remedial scheme for illustrative example III.

Action Type and Location	Time (s)	Action Magnitude
TSA detection	1.3167	*delP*=682.049 MW
Trip G 38	1.3667	Shed 830 MW Power Generation
Shed All Loads	1.4167	Shed proportionate % load illustrated in Figure 22(a) with total load shed equal to *delP*

In this condition, the inverter remains connected to the power grid and delivers the requisite amount of reactive current during the time of grid faults with zero real current injection. The control model as shown in Fig. 13 (b), which is considered in this work, enhances the active power recovery capability and other essential parameters, thus improving the fault ride through capability.

Following the solar energy integration, the system operates within permissible frequency settings of about 60 Hz nominal frequency (flow(norm) = 59.9 Hz, fhigh(norm) = 60.1 Hz) [26]. However, with solar energy penetration, the system inertia decreases, and it is highlighted in Fig. 14. The decreased inertia indicates a reduced time-margin to sustain system frequency within operating limits until control settings are initiated. The performance of the proposed strategy enabling real-time emergency control of modified test system is demonstrated with the following illustrative example.

1) ILLUSTRATIVE EXAMPLE II

At System Loading 98% of base case and 10.72% solar energy penetration, Short Circuit fault occurred near Bus 02, FAT=1s; Cleared by opening Line 02-25, FCT=1.2s.=

This scenario reflects a response of the SE penetrated test system when subjected to a disturbance as shown in Fig. 15. The figure also displays the Bus 32 (solar energy source) voltage magnitude and angle response for the considered disturbance. Subsequent to the fault clearance, within one second, G37 and G38 generators are out-of-step. The arisen instability is then propagated in whole system and can be visualized via the system load voltage profile. The proposed PIE assess the system to be unstable and time to initiate remedial strategy. The application of DAAC suggests load shedding equal to the estimated power imbalance in the system, viz. 600.334 MW. The recommendations of the strategy are tabulated in Table 5. The distribution of % load shedding among different loads is calculated and illustrated in Fig. 16 (a). Moreover, Fig. 16 (b) displays the total system load for pre and post deployment of strategy with active (MW) and quadrature (MVAr) components. The application results in Fig. 17 showcase the successful implementation of the proposed method in controlling system stability and enhancing grid performance even in the presence of SE penetration. The post-emergency control system performance is shown via the average load profile, generator node angles, and solar penetration site voltage profile.

D. TEST RESULTS OF THE MULTIPLE LOCATIONS SOLAR ENERGY INTEGRATED POWER SYSTEM

The capability of the proposed composite scheme is further tested on the New England 39 bus test system modified with multiple solar plants replacing conventional generators at

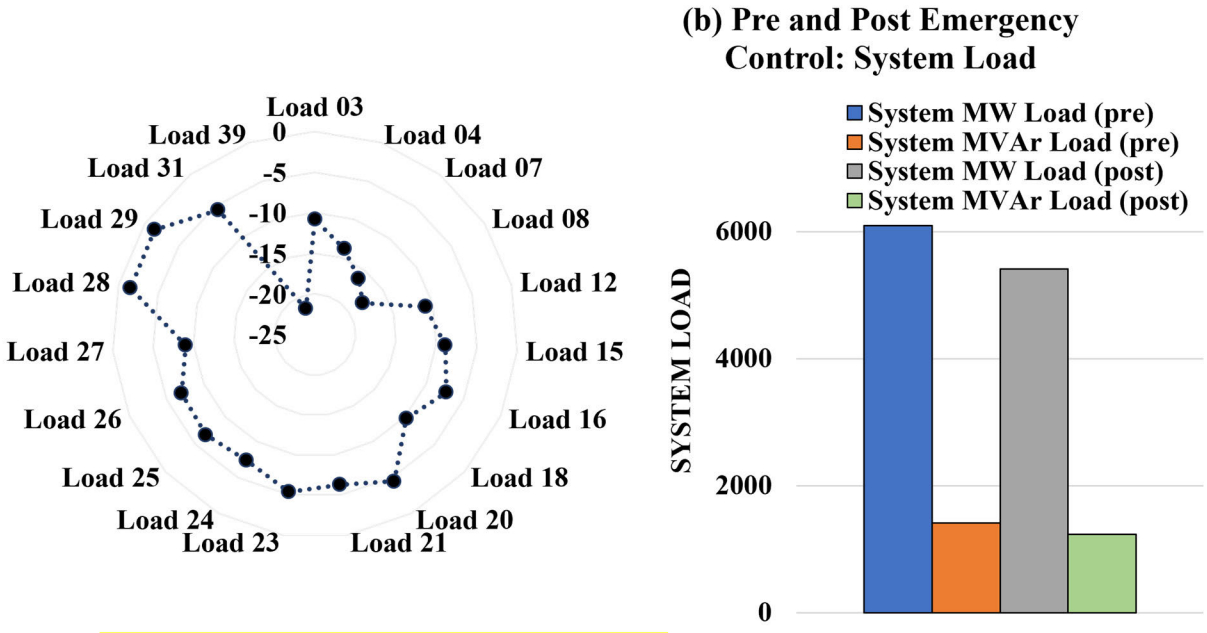

FIGURE 21. Illustrative Example III: load shedding post generation.

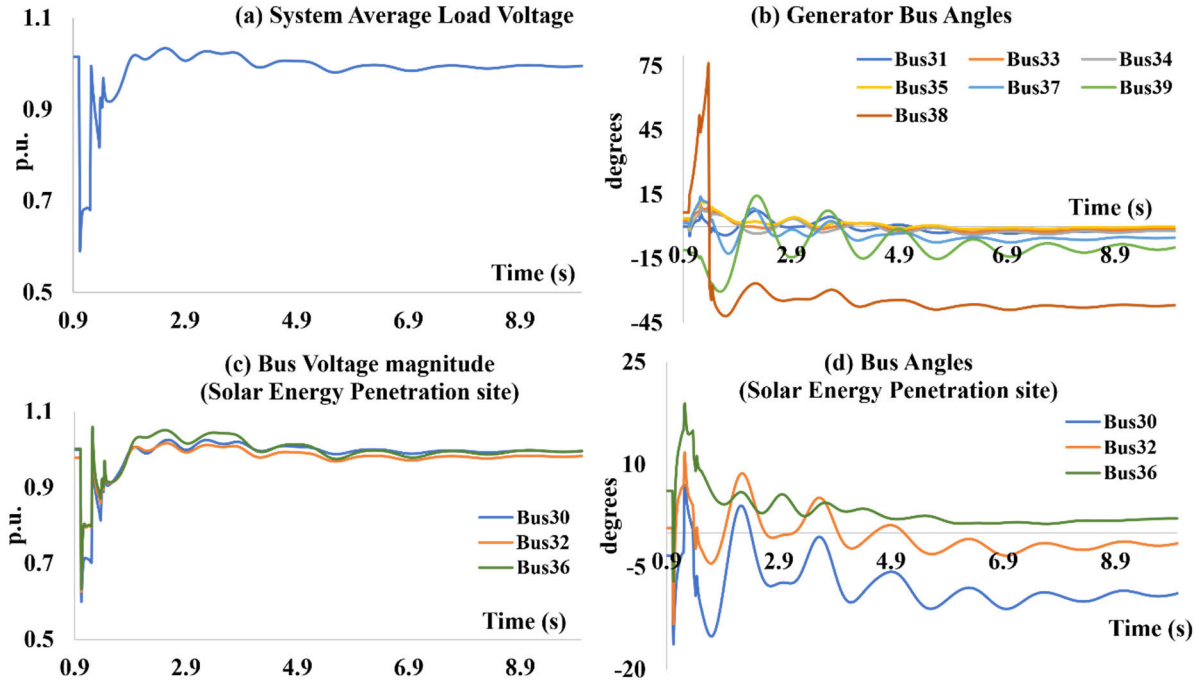

FIGURE 22. Illustrative Example III: with emergency remedial strategy.

Bus 30, Bus 32, and Bus 36, as shown in Fig. 18. A solar PV farm rated at 330 MVA is located at Bus 30, 660 MVA is located at Bus 32, and 550 MVA is located at Bus 36. However, the multiple solar energy penetration decreases system inertia further than that of single site penetration, as shown in Fig. 19. The proposed strategy enabling real-time emergency control of the modified test system with SE penetration at multiple buses is demonstrated with Illustrative Example III.

1) ILLUSTRATIVE EXAMPLE III

At 100% System Loading and 22.795 % solar energy penetration, Short Circuit fault occurred at Line 26-28, FAT=1s, Location= 50%; Cleared by opening Line 26-28, FCT=1.2s.

The example III demonstrates another effective application of the proposed scheme on increased solar energy integrated test system when subjected to a disturbance. The network response for ensuing event is shown in Fig. 20. Post-fault

TABLE 7. Performance comparison of proposed work.

Scheme	Solar Energy Penetration	Prompt Stability Evaluation		Type of Emergency Measures			Nature of Enhanced Grid Operation	Type of Execution
		%FA	%MA	GR	LSPGR	LS		
[17]	No	2.467	1.405	Generator Out	≥ *delp*	≥ *delp*	Transient Stability	Real-Time
[26]	~2.5 % (Single bus: 147 MW)	NA	NA	NA	NA	*delP* (stepwise)	Frequency Stability	Online
[31]	No	NA	NA	Generator Out	NA	NA	Transient Stability	Real-Time
Proposed	**~22.8% (Multiple bus: 1400 MW)**	**3.78**	**0**	**Generator Out**	***delP* (DRBI)**	***delP* (DRBI)**	**Transient Stability**	**Real-Time**

FA: False alarm; MA: Missed alarm; GR: Generator rejection; LSPGR: load shedding post-generator rejection; LS: Load shedding; NA: Not available/applicable

clearance, with course of time, initially, generator G38 is most advanced against the rest of the system and is out-of-step by around 1.55 seconds. Subsequently, this instability is propagated to the rest of the system, and the grid collapses. It is therefore important to assess the impending instability state and apply remedial solutions to avert the grid failure. The prompt TSA assessment, post-assessment action type judgement, time of initiation, and action magnitude are tabulated in Table 6. As generator G38 is accelerating more than other generators and driving other machines to slow down more, it is appropriate to trip the generator. As G38 tripping adds to the power imbalance, load shedding corresponding to the estimated imbalance is necessary. Load Sharing Index estimates suggest an adequate magnitude of load shedding from all the loads essentially in proportion to the 682.049 MW power imbalance. The distribution of % load shedding among different loads is calculated and illustrated in Fig. 21 (a).

Moreover, Fig. 21 (b) displays the total system load for pre and post deployment of a strategy with active (MW) and quadrature (MVAr) components. A delay of 3 cycle in generator trip and 3 cycle delay (total 6 cycle) in subsequent load shedding are considered to allow different associated delays. The application results in Fig. 22 showcase the successful implementation of the proposed methodology in controlling system stability and enhancing the grid performance even in the presence of SE penetration at multiple locations. The post-emergency control system performance is shown via the average load profile, generator node angles, and solar penetration site voltage profile.

E. COMPARATIVE ASSESSMENT OF THE PROPOSED FRAMEWORK

The performance of the proposed method has been further validated through a comparison with the present state of the art. Investigations on the transient stability assessment and effective deployment of emergency control mechanisms for these solar energy integrated systems is relatively rare. Therefore, we have considered following references [17], [26] and [31] for the comparisons which empirically contributes similar to that of this article. Table 7 showcases the superiority of the proposed scheme with respect to considered references. The attributes considered for the evaluation are: (1) solar energy penetration in the grid, (2) false and missed alarms of real-time stability assessment, (3) types of emergency measures and their magnitude, (4) nature of enhanced grid operation and (5) type of execution. Evidently, the proposed scheme flags prompt TSA assessment with zero missed alarms, very few false alarms, computes the action type, location, and magnitude of emergency strategy in real time with minimum computation burden. Additionally, the presented method is suitable for both the power systems: conventional grids and grids with solar energy penetration at single and multiple buses.

V. CONCLUSION

In the scenario of increased power demand, the grid operators are poised to increase renewable energy penetration. The increased generation combination impels the centralized control centers to effectively monitor and perform vulnerability assessment. Grid control centers are required to identify and implement the intended emergency control measures and improve grid sustainability based on the assessments. Essentially, these measures are required to be insensitive to renewable energy generation in the grid. In view of it following contributions has been accomplished in this article:

1. A unified approach that ensures system synchronism in a solar integrated power network by first assessing the imminent susceptibility, then preparing and deploying the emergency scheme is presented effectively.

2. To determine when corrective action should be taken and to evaluate the impending transient instability of the system in the presence of SE, the EWMA treated short-moving synchronized data window of power generated from the sources is employed.

3. A DAAC based emergency corrective technique is implemented to maintain the system's transient stability and improve grid performance in real-time. The DAAC utilizes DRBI to assess the action set comprising of action type, location, and magnitude of actions.

The scheme is tested on New England 39 Bus test system in the absence and presence of SE. The expediency of the unified strategy in enhancing grid performance even in the presence of single and multiple solar energy farms

is highlighted. A comparative performance of the proposed work with the available state-of-art establishes the utility of the projected scheme.

ACKNOWLEDGMENT

The authors extend their appreciation to the Researchers Supporting Project at King Saud University, Riyadh, Saudi Arabia, for funding this research work through the project number RSP2023R278. The authors would like to acknowledge the technical support from Intelligent Prognostic Private Ltd., Delhi, India, researcher's supporting Project for this research work. The authors would like to acknowledge the technical support from Ingenium Research Group, Universidad Castilla-La Mancha, Ciudad Real, Spain. They would also like to thank the Power System Laboratory, Electrical Engineering Department, Manipal University, Jaipur, for giving them the opportunity to utilize the software facility.

REFERENCES

[1] M. Kezunovic, J. D. McCalley, and T. J. Overbye, "Smart grids and beyond: Achieving the full potential of electricity systems," *Proc. IEEE*, vol. 100, no. Special Centennial Issue, pp. 1329–1341, May 2012, doi: 10.1109/JPROC.2012.2187131.

[2] M. Begovic, D. Novosel, D. Karlsson, C. Henville, and G. Michel, "Wide-area protection and emergency control," *Proc. IEEE*, vol. 93, no. 5, pp. 876–891, May 2005, doi: 10.1109/JPROC.2005.847258.

[3] P. Tielens and D. Van Hertem, "The relevance of inertia in power systems," *Renew. Sustain. Energy Rev.*, vol. 55, pp. 999–1009, Mar. 2016, doi: 10.1016/j.rser.2015.11.016.

[4] S. M. Mazhari, B. Khorramdel, C. Y. Chung, I. Kamwa, and D. Novosel, "A simulation-based classification approach for online prediction of generator dynamic behavior under multiple large disturbances," *IEEE Trans. Power Syst.*, vol. 36, no. 2, pp. 1217–1228, Mar. 2021, doi: 10.1109/TPWRS.2020.3021137.

[5] D. R. Shrivastava, S. A. Siddiqui, and K. Verma, "Model free robust real-time severity analyser using PMU measurements," *Int. J. Electr. Power Energy Syst.*, vol. 133, Dec. 2021, Art. no. 107333, doi: 10.1016/j.ijepes.2021.107333.

[6] A. Sajadi, R. Preece, and J. Milanovic, "Identification of transient stability boundaries for power systems with multidimensional uncertainties using index-specific parametric space," *Int. J. Electr. Power Energy Syst.*, vol. 123, Dec. 2020, Art. no. 106152, doi: 10.1016/j.ijepes.2020.106152.

[7] X. Liu, Y. Min, L. Chen, X. Zhang, and C. Feng, "Data-driven transient stability assessment based on kernel regression and distance metric learning," *J. Modern Power Syst. Clean Energy*, vol. 9, no. 1, pp. 27–36, Jan. 2021, doi: 10.35833/MPCE.2019.000581.

[8] Y. J. Isbeih, M. S. El Moursi, W. Xiao, and E. El-Saadany, "Generator-based threshold for transient stability assessment," *IET Smart Grid*, vol. 2, no. 3, pp. 407–419, Sep. 2019, doi: 10.1049/iet-stg.2018.0292.

[9] H. Cui, Q. Wang, Y. Ye, Y. Tang, and Z. Lin, "A combinational transfer learning framework for online transient stability prediction," *Sustain. Energy, Grids Netw.*, vol. 30, Jun. 2022, Art. no. 100674, doi: 10.1016/j.segan.2022.100674.

[10] H. Wang and S. Wu, "Transient stability assessment with time-adaptive method based on spatial distribution," *Int. J. Electr. Power Energy Syst.*, vol. 143, Dec. 2022, Art. no. 108464, doi: 10.1016/j.ijepes.2022.108464.

[11] G. Wang, J. Guo, S. Ma, X. Zhang, Q. Guo, S. Fan, and H. Xu, "Data-driven transient stability assessment with sparse PMU sampling and online self-check function," *CSEE J. Power Energy Syst.*, vol. 9, no. 3, pp. 910–920, May 2022, doi: 10.17775/CSEEJPES.2021.05890.

[12] B. Li and J. Wu, "Adaptive assessment of power system transient stability based on active transfer learning with deep belief network," *IEEE Trans. Autom. Sci. Eng.*, vol. 20, no. 2, pp. 1047–1058, Apr. 2023, doi: 10.1109/TASE.2022.3181029.

[13] S. Wu, L. Zheng, W. Hu, R. Yu, and B. Liu, "Improved deep belief network and model interpretation method for power system transient stability assessment," *J. Modern Power Syst. Clean Energy*, vol. 8, no. 1, pp. 27–37, Jan. 2020, doi: 10.35833/MPCE.2019.000058.

[14] Y. Liu, J. Wang, and Z. Yue, "Improved multi-point estimation method based probabilistic transient stability assessment for power system with wind power," *Int. J. Electr. Power Energy Syst.*, vol. 142, Nov. 2022, Art. no. 108283, doi: 10.1016/j.ijepes.2022.108283.

[15] M. Q. Ahsan, A. H. Chowdhury, S. S. Ahmed, I. H. Bhuyan, M. A. Haque, and H. Rahman, "Technique to develop auto load shedding and islanding scheme to prevent power system blackout," *IEEE Trans. Power Syst.*, vol. 27, no. 1, pp. 198–205, Feb. 2012, doi: 10.1109/TPWRS.2011.2158594.

[16] M. A. Kabir, A. H. Chowdhury, and N. A. Masood, "A dynamic-adaptive load shedding methodology to improve frequency resilience of power systems," *Int. J. Elect. Power Energy Syst.*, vol. 122, Nov. 2020, Art. no. 106169, doi: 10.1016/j.ijepes.2020.106169.

[17] S. A. Siddiqui, K. Verma, K. R. Niazi, and M. Fozdar, "A unified control scheme for power system transient stability enhancement through preventive and emergency control," *Int. Trans. Electr. Energy Syst.*, vol. 26, no. 2, pp. 365–383, Feb. 2016, doi: 10.1002/etep.2086.

[18] T. Shekari, A. Gholami, F. Aminifar, and M. Sanaye-Pasand, "An adaptive wide-area load shedding scheme incorporating power system real-time limitations," *IEEE Syst. J.*, vol. 12, no. 1, pp. 759–767, Mar. 2018, doi: 10.1109/JSYST.2016.2535170.

[19] J. Tang, J. Liu, F. Ponci, and A. Monti, "Adaptive load shedding based on combined frequency and voltage stability assessment using synchrophasor measurements," *IEEE Trans. Power Syst.*, vol. 28, no. 2, pp. 2035–2047, May 2013, doi: 10.1109/TPWRS.2013.2241794.

[20] D. S. Kumar, A. Sharma, D. Srinivasan, and T. Reindl, "Stability implications of bulk power networks with large scale PVs," *Energy*, vol. 187, Nov. 2019, Art. no. 115927, doi: 10.1016/j.energy.2019.115927.

[21] B. B. Adetokun, J. O. Ojo, and C. M. Muriithi, "Application of large-scale grid-connected solar photovoltaic system for voltage stability improvement of weak national grids," *Sci. Rep.*, vol. 11, no. 1, Dec. 2021, Art. no. 24526, doi: 10.1038/s41598-021-04300-w.

[22] S. R. Paital, P. K. Ray, A. Mohanty, and S. Dash, "Stability improvement in solar PV integrated power system using quasi-differential search optimized SVC controller," *Optik*, vol. 170, pp. 420–430, Oct. 2018, doi: 10.1016/j.ijleo.2018.05.097.

[23] R. G. Wandhare and V. Agarwal, "Novel stability enhancing control strategy for centralized PV-grid systems for smart grid applications," *IEEE Trans. Smart Grid*, vol. 5, no. 3, pp. 1389–1396, May 2014, doi: 10.1109/TSG.2013.2279605.

[24] M. K. Hossain and M. H. Ali, "Transient stability augmentation of PV/DFIG/SG-based hybrid power system by parallel-resonance bridge fault current limiter," *Electr. Power Syst. Res.*, vol. 130, pp. 89–102, Jan. 2016, doi: 10.1016/j.epsr.2015.08.016.

[25] A. Jawad, S. A. Naim, C. Saha, and N.-A. Masood, "Frequency stability enhancement of a large-scale PV integrated grid," in *Proc. 11th Int. Conf. Electr. Comput. Eng. (ICECE)*, Dec. 2020, pp. 290–293.

[26] A. Chandra and A. K. Pradhan, "An adaptive underfrequency load shedding scheme in the presence of solar photovoltaic plants," *IEEE Syst. J.*, vol. 15, no. 1, pp. 1235–1244, Mar. 2021, doi: 10.1109/JSYST.2020.2995050.

[27] S.-Y. Kuo and Y.-H. Chou, "Building intelligent moving average-based stock trading system using metaheuristic algorithms," *IEEE Access*, vol. 9, pp. 140383–140396, 2021, doi: 10.1109/ACCESS.2021.3119041.

[28] M. B. Perry, "The exponentially weighted moving average," in *Wiley Encyclopedia of Operations Research and Management Science*. Hoboken, NJ, USA: Wiley, 2011, doi: 10.1002/9780470400531.eorms0314.

[29] P. Bhui and N. Senroy, "Real-time prediction and control of transient stability using transient energy function," *IEEE Trans. Power Syst.*, vol. 32, no. 2, pp. 923–934, Mar. 2017, doi: 10.1109/TPWRS.2016.2564444.

[30] G. Lammert, L. D. P. Ospina, P. Pourbeik, D. Fetzer, and M. Braun, "Implementation and validation of WECC generic photovoltaic system models in DIgSILENT PowerFactory," in *Proc. IEEE Power Energy Soc. Gen. Meeting (PESGM)*, Jul. 2016, pp. 1–5.

[31] Y. Zhang, M. Pavella, and L. Wehenkel, "A method for real-time transient stability emergency control," *IFAC Proc. Volumes*, vol. vol., 30, no. 17, pp. 633–638, 1997, doi: 10.1016/S1474-6670(17)46476-7.